Marine and Petroleum Geology 182 (2025) 107592

Contents lists available at ScienceDirect

Marine and Petroleum Geology

journal homepage: www.elsevier.com/locate/marpetgeo

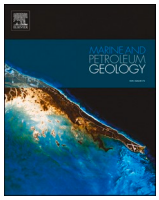

Diagenesis and burial history controls on Oligocene Huagang sandstones, southern Xihu Sag (East China Sea Basin): Implications for the formation of effective reservoirs

Hong-Liang Huo [a,b], Cheng-Lin Liu [a,b,*], Dao-Wu Huang [c], An-Qi Tian [a,b], Rizwan Sarwar Awan [d], Hong-Yan Gao [c], Chuang-Xin Liu [c], Xue-Yong Chen [a,b], Zi-Ye Tian [a,b], Tao-Zheng Yang [a,b], Bin-Bin Liu [c], Chao-Jun Liang [e]

[a] State Key Laboratory of Petroleum Resources and Engineering, China University of Petroleum (Beijing), Beijing, 102249, China
[b] College of Geosciences, China University of Petroleum-Beijing, Beijing, 102249, China
[c] Shanghai Branch of China National Offshore Oil Corporation Ltd., Shanghai, 200050, China
[d] Institute of Unconventional Oil & Gas, Northeast Petroleum University, Daqing, 163318, China
[e] Sinopec International Petroleum Exploration and Development Corporation, Beijing, 100029, China

ARTICLE INFO

Keywords:
Diagenetic evolution
Controlling factor
Reservoir quality
Effective reservoir
Huagang Formation
Xihu Sag

ABSTRACT

This study aims to reveal the diagenetic evolution sequence and controlling factors of Oligocene Huagang Formation (E_3h) sandstone reservoirs in the HY area, and predict high-quality reservoir distribution to guide hydrocarbon exploration. A comprehensive approach integrating core observation, thin-section petrography, geochemical analysis, and seismic-log interpretation was employed. By combining burial history simulation and diagenetic analysis, we systematically analyzed reservoir quality and diagenetic evolution and established evolution models for effective reservoir pore spaces. Results indicate that E_3h sandstones underwent intense diagenetic processes including compaction, cementation, and dissolution. Diagenesis plays a critical role in controlling reservoir quality: compaction is the primary factor that governs vertical variations in petrophysical properties, where shallower intervals typically exhibit better quality than deeper ones. In contrast, cementation and dissolution serve as secondary controls, explaining property differences between Blocks A and B, with Block A reservoirs being superior. A three-stage relationship has been identified between burial history and diagenesis: (1) early gradual subsidence stage (GSS) with weak feldspar dissolution, early carbonate cementation, chlorite coating, and mechanical compaction; (2) intermediate tectonic activity stage (TAS) with massive feldspar dissolution, quartz overgrowth precipitation, and ferruginous cement formation; (3) late stable burial stage (SBS) featuring intensified compaction and clay mineral transformations. The spatial configuration of fault systems and sandstones, combined with compositional attributes, strongly controls diagenetic evolution. Favorable zones for dissolution development occur at intersections of fault zones and acidic fluid migration pathways, while quartz-feldspar-rich zones mitigate porosity loss via compaction resistance. Three effective reservoir development models were proposed: high dissolution-low cementation-low compaction, moderate dissolution-low cementation-low compaction, and low compaction-low cementation-low dissolution. This research provides a critical basis for predicting E_3h high-quality reservoirs in the study area. Furthermore, the comprehensive burial history-diagenesis analysis method presented here offers a valuable reference for studies on sandstone diagenetic evolution and hydrocarbon exploration in similar geological settings.

1. Introduction

Sandstone reservoirs serve as critical carriers for hydrocarbon exploration and development, with their reservoir properties directly influencing hydrocarbon occurrence and exploitation efficiency (Radwan et al., 2022; Feng et al., 2023; Marghani et al., 2023). Diagenesis, as a key factor controlling sandstone reservoir quality, has long been the focus of research in the geological community (Bjørlykke,

* Corresponding author. College of Geosciences, China University of Petroleum (Beijing), Beijing, 102249, China.
E-mail addresses: 15010065116@163.com (H.-L. Huo), lclzgx@126.com (C.-L. Liu).

https://doi.org/10.1016/j.marpetgeo.2025.107592
Received 25 April 2025; Received in revised form 8 August 2025; Accepted 28 August 2025
Available online 29 August 2025

2014; Zhang et al., 2022; Bello et al., 2024; Huo et al., 2025). Previous research indicates that diagenesis involves multiple processes, including compaction, cementation, and dissolution (Higgs et al., 2007; Morad et al., 2010; Qian et al., 2020). These processes exert decisive control over the evolution of sandstone pore structures and petrophysical properties. Compaction reduces primary porosity through particle rearrangement and plastic deformation (Zhang et al., 2015; Wang et al., 2019). Cementation further decreases reservoir permeability by filling pores with precipitated cements such as calcite and quartz. Conversely, dissolution can create secondary porosity under specific conditions. It improves reservoir quality by dissolving framework grains or cement matrices (Xi et al., 2019; Radwan et al., 2022).

Burial history studies have revealed the subsidence-uplift processes of strata throughout geological time and their profound influence on diagenesis and reservoir quality (Wang et al., 2020; Bah et al., 2023; Liu et al., 2024). Variations in burial depth regulate temperature-pressure regimes, thereby controlling diagenetic reaction rates and outcomes (Faiz et al., 2007; Zhang et al., 2022; Chen et al., 2024). Deep burial under high-temperature/high-pressure conditions accelerates compaction and cementation, degrading reservoir properties. In contrast, tectonic uplift-induced decompression and fluid migration may initiate dissolution events that rejuvenate reservoir quality (Poursoltani et al., 2019; Wang et al., 2020; Tamburelli et al., 2022). This dynamic interplay between burial history and diagenesis exhibits regional variability, resulting in complex spatiotemporal patterns of reservoir quality development (Bjørlykke, 2014; Blamey et al., 2014).

The sandstone reservoirs of E_3h in the southern Xihu Sag of the East China Sea Basin are significant hydrocarbon exploration targets (Abbas et al., 2018; Wang et al., 2022; Zhang et al., 2023; Yang et al., 2024). Previous studies have laid a foundation, yet critical unresolved issues persist. First, the characteristics and evolutionary processes of diagenesis in E_3h sandstones remain unclear, particularly the superimposition and competition among multiple diagenetic processes and their impacts on pore evolution (Wang et al., 2021; Zeng et al., 2021). Additionally, while the importance of diagenesis and burial history to E_3h reservoir quality is recognized, the specific control models of their coupled relationships on effective reservoir formation remain undefined. This severely restricts the accurate prediction of effective reservoir distribution patterns in the region (Wang et al., 2020; Zhang et al., 2022). Therefore, further research on diagenesis and burial history in E_3h sandstones is crucial for revealing effective reservoir formation mechanisms and guiding hydrocarbon exploration.

Taking the sandstone reservoirs of the E_3h in the southern Xihu Sag as a case study, this research employs methods including thin-section analysis, scanning electron microscopy (SEM), mineral composition analysis, routine core analysis, fluid inclusion studies, and carbonate carbon-oxygen isotope analysis. The objectives are to: 1) characterize diagenetic types, intensities, and evolutionary sequences; 2) evaluate the coupled relationships between diagenesis and burial history and their impacts on reservoir quality. Additionally, through integrated analysis of diagenetic types, intensities, and evolutionary sequences in sandstone reservoirs, an effective reservoir formation model based on burial history, fault system, and diagenesis is established. This study provides scientific and technical support for hydrocarbon exploration and development in the region.

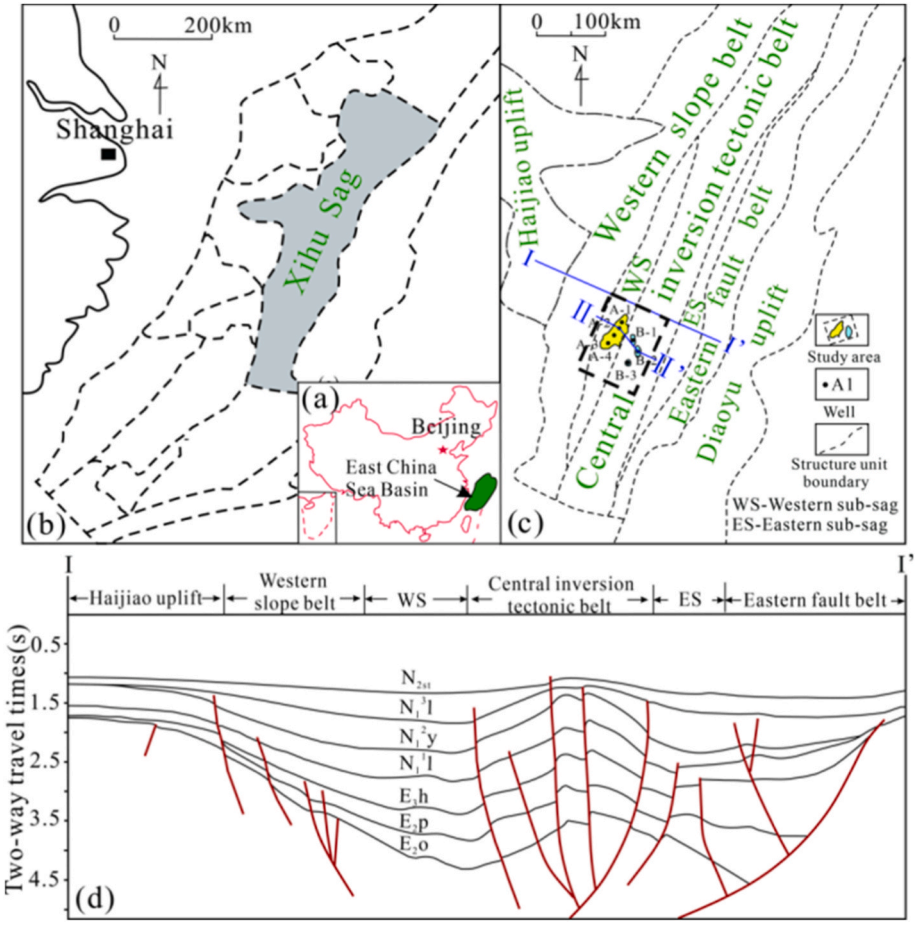

Fig. 1. (a) Geographical location of the East China Sea Basin; (b) Tectonic location of the Xihu Sag; (c) Location of the study area and well distribution (modified after (Wang et al., 2020)); (d) Seismic profile of the Ningbo tectonic belt (modified after (Wang et al., 2020)).

2. Geological setting of the Huagang Formation

The Xihu Sag is an elongated NE-trending Cenozoic sedimentary sag and serves as a major hydrocarbon-producing base within the East China Sea Basin (Fig. 1a–b) (Zhu et al., 2019; Zhang et al., 2020). From west to east, the Xihu Sag can be divided into five tectonic units: Western slope belt, Western sub-sag, Central uplift belt, Eastern sub-sag, and Eastern sharp slope (Fig. 1c and d) (Wang et al., 2020; Yang et al., 2024). The study area (HY area) is situated in the central-southern Xihu Sag, encompassing Well block A and Well block B. Tectonically spanning both the Western sub-sag and Central inversion tectonic belt, this region harbors abundant hydrocarbon resources.

The Xihu Sag contains extremely thick Cenozoic sedimentary strata, which from bottom to top consist of the Eocene Pinghu formation (E_2p), Oligocene Huagang formation (E_3h), Miocene Longjing (N_1^1l), Yuquan (N_1^2y), and Liulang (N_1^3l) formations, Pliocene Santan (N_{2st}) Formation, and Quaternary Donghai Group (Qd) (Fig. 2) (Qian et al., 2020, 2022). The E_3h serves as a key hydrocarbon exploration target in the Xihu Sag and can be further divided into H1-H12 members from top to bottom (Hao et al., 2018; Ma et al., 2025). Specifically, the Huagang Formation is subdivided into two sub-members based on lithological and sedimentary characteristics: E_3hs (upper sub-member of the Huagang Formation) comprises H1 to H5, while E_3hx (lower sub-member of the Huagang Formation) includes H6 to H12 (Fig. 2). During the deposition of the E_3h, the Xihu Sag was in a shallow-water delta sedimentary environment where fluvial systems transported abundant terrigenous clastic materials, forming widespread sandstone, siltstone, and mudstone depositional associations (Hao et al., 2018; Ma et al., 2025). The E_3h experienced multiple tectonic movements, with the Late Miocene Longjing Movement being the most significant, causing intense stratigraphic uplift, erosion, folding, and thrust faulting (Ma et al., 2025). The E_3h in the study area has a sedimentary thickness of 800 m–1600 m and a burial depth ranging from 2200 m to 4400 m.

3. Samples and data analysis

3.1. Samples

This study focuses on the sandstones of the E_3h in the HY Block of the southern Xihu Sag. Based on observations of 145.7 m of cores from seven wells in the Xihu Sag (Table 1), representative core and cutting samples were selected to analyze reservoir diagenesis and quality. All samples, seismic data, logging, most porosity/permeability data, and thin-section data were provided by the Shanghai Branch of China National Offshore Oil Corporation (CNOOC). The study samples were collected from deep reservoirs in the central-northern Xihu Sag, with burial depths ranging from 3200 to 4400 m, and derived from seven wells: A-1, A-2, A-3, A-4, B-1, B-2, and B-3 (Fig. 1c). All data were utilized to investigate the

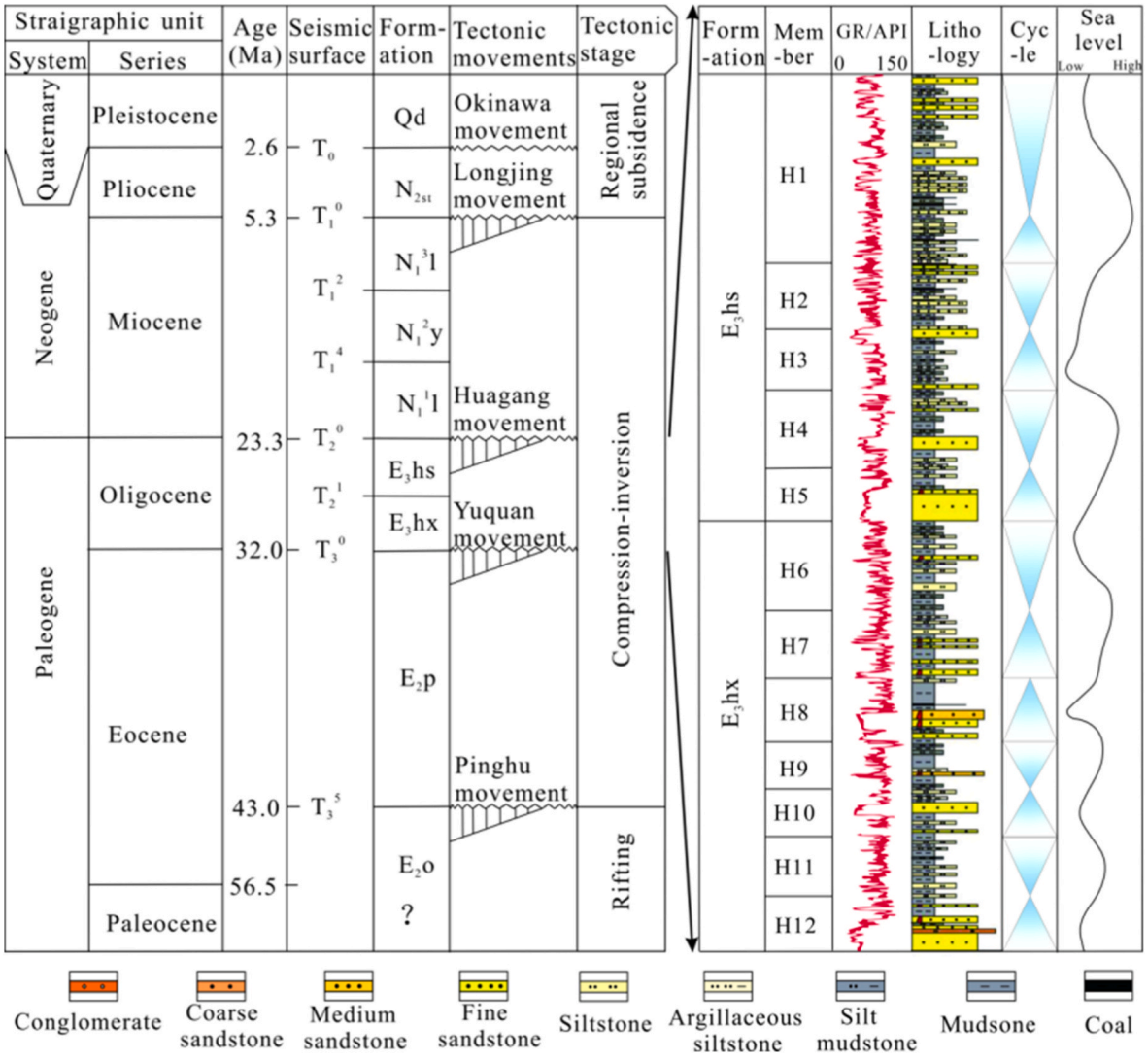

Fig. 2. Stratigraphic composition of the study area and stratigraphic characteristics of E_3h (modified after Qian et al., 2020).

Table 1
Core data statistics.

Sag	Formation	Well	Member	Depth (m)
Xihu	E_3h	A-1	H5	3524–3542 m
Xihu	E_3h	A-2	H8	3958–3968 m
Xihu	E_3h	A-2	H11	4184–4202 m
Xihu	E_3h	A-3	H5	3862–3879 m
Xihu	E_3h	A-4	H5	3645–3659 m
Xihu	E_3h	B-1	H2	3291–3298 m
Xihu	E_3h	B-1	H8	3931–3940 m
Xihu	E_3h	B-2	H3	3420–3429 m
Xihu	E_3h	B-3	H5	3654–3663 m
Xihu	E_3h	B-3	H11	4185–4197 m

diagenetic evolution of E_3h sandstone in the HY area.

3.2. Experimental methods

To analyze the diagenetic processes and reservoir quality control factors, multiple technical approaches were employed, including optical microscopy, SEM, scanning electron microscopy-cathodoluminescence (SEM-CL), X-ray diffraction (XRD), high-pressure mercury intrusion (HPMI), carbon-oxygen isotope analysis, and fluid inclusion experiments. These methods were applied to investigate the mineral composition, diagenetic characteristics, and pore evolution of the reservoir in the study area.

Optical microscopy and cast thin sections with SEM-CL observations were used to analyze detrital components, pore types, and cementation sequences (Bello et al., 2024). Mineralogical features, pore types, and their abundances were quantified using the point counting method. XRD analysis was conducted using a Bruker D8 Advance diffractometer (5–60° diffraction angle, 40 kV) to identify clay mineral types and abundances, with a focus on illite, kaolinite, and carbonate cements critical for evaluating burial diagenesis (Li et al., 2022). SEM observations were performed on freshly broken, gold-coated core samples using an FEI Quanta 200 microscope (15 kV accelerating voltage, 5 nm resolution) to characterize microscopic diagenetic textures and determine the development and distribution of key diagenetic minerals (Goldstein et al., 2017). Fluid inclusion analysis employed a Linkam THMS600 heating-freezing stage to measure homogenization and ice-melting temperatures of fluid inclusions in minerals, constraining cementation temperatures and paleofluid salinity (Xi et al., 2015). Carbon-oxygen isotope analysis of carbonate cements was conducted using a Finnigan MAT 253 mass spectrometer. Samples were reacted with phosphoric acid at 70 °C, and isotopic ratios were calibrated against NBS-18/NBS-19 standards. Results are reported as per mil deviations relative to the Pee Dee Belemnite (PDB) standard, with an analytical precision of ±0.22 ‰ (El-Ghali et al., 2024). HPMI experiments were carried out using an AutoPore IV 9505 mercury porosimeter (maximum intrusion pressure: 200 MPa) following the Chinese National Standard GB/T 29171–2012 to evaluate pore-throat characteristics of reservoir samples (Lai et al., 2016).

Based on published literature data (denudation amounts, timing of thermal events, etc.) (Xu et al., 2020; Zhou et al., 2020), the burial history of E_3h was reconstructed using PetroMod v2016 software, incorporating core, logging, and seismic data collected from typical cored wells of Shanghai Branch of CNOOC Ltd. Modeling parameters, including stratigraphic burial depth, lithology, reservoir thickness, formation temperature, and vitrinite reflectance (Ro), were provided by the Shanghai Branch. Other conditions, such as heat flow, erosion thickness, and source rock data, were derived from published literature. Average total organic carbon (TOC) values for Eocene E_2p dark mudstones and coals are 1.31 wt% and 61.8 wt%, respectively. The hydrocarbon generation potentials of dark mudstones and coals are 200 mg/g and 226 mg/g, respectively (Xie et al., 2015). Kinetic parameters for Type III kerogen incorporated into the basin modeling software were adopted (Behar et al., 1997; Wang et al., 2020).

4. Results

4.1. Petrological characteristics

Based on observations and statistics from over 200 thin sections in the study area, the detrital composition of E_3h sandstones is characterized by quartz (55 %–82 %), feldspar (10 %–28 %), and lithic fragments (8 %–25 %). According to Folk's (Folk, 1980) classification (Fig. 3), the dominant rock type is feldspathic litharenite, with minor occurrences of lithic arkose, subarkose, and sublitharenite. Quartz, the primary component, appears as both monocrystalline and polycrystalline varieties. Lithic fragments include igneous (extrusive and granite), metamorphic, and sedimentary (mudstone and sandstone) lithologies. The E_3h sandstones demonstrate high compositional maturity, with Quartz/(Feldspar + Rock fragment) ratios ranging from 1.59 to 2.40.

Based on the identification data of cast thin sections, the matrix content of E_3h reservoirs in the study area averages 8.06 %, predominantly composed of carbonate cements and argillaceous matrix, with subordinate calcareous cements and occasional siliceous cements. The argillaceous matrix averages 1.37 %, mainly consisting of mudstone clasts with uneven distribution, locally enriched in layered, banded, or nodular forms and displaying significant recrystallization. Total cement content averages 6.68 %, including calcite, dolomite, ankerite, silica, and clay minerals. Among these, clay minerals represent the most abundant cement type with an average content of 2.97 %. Carbonate cements rank second in abundance, averaging 3.14 % and accounting for approximately 40 % of the total cement content. Siliceous cements are generally scarce in the study area, with contents less than 1 % (Fig. 3).

4.2. Pore types and characteristics

Thin-section observations and SEM analysis identify four main types of fluid storage spaces in E_3h reservoirs: primary intergranular pores, intergranular dissolution pores, intragranular dissolution pores, and intercrystalline pores. Primary intergranular pores form between detrital grains during deposition. They are often reduced by compaction or partially/fully filled with cement. The currently observed pores are mainly residual primary intergranular pores, which are triangular or polygonal in shape with straight edges and uneven distribution (Fig. 4a). Intergranular and intragranular dissolution pores are the dominant secondary pore types. Intragranular dissolution pores include two main categories: feldspar dissolution pores and lithic dissolution pores (Fig. 4b and c). Feldspar dissolution pores are characterized by dissolution along the cleavage planes of perthite and albite. Lithic dissolution pores consist of small dissolved cavities within acidic volcanic fragments and andesite debris. When detrital grains are completely dissolved, moldic pores form, where only the outline of the original grain and residual insoluble components remain visible under the microscope. These pores are low in abundance but typically large in size (Fig. 4d). Additionally, composite pores with larger diameters can form when residual primary intergranular pores are enlarged by subsequent dissolution (Fig. 4d). Intercrystalline pores are primarily observed between authigenic kaolinite crystals, illite, and chlorite grains (Fig. 4e and f). These pores have low abundance and smaller diameters (<0.5 μm).

4.3. Diagenesis characteristics

4.3.1. Compaction

Petrographic analysis of E_3h samples indicates that the reservoirs in the study area experienced intense compaction, characterized by closely packed grain arrangements with dominant point-line contacts and subordinate line-concave contacts (Fig. 5a–c, f). Grain reorientation under overburden pressure led to preferential orientation (Fig. 5b–e). Under

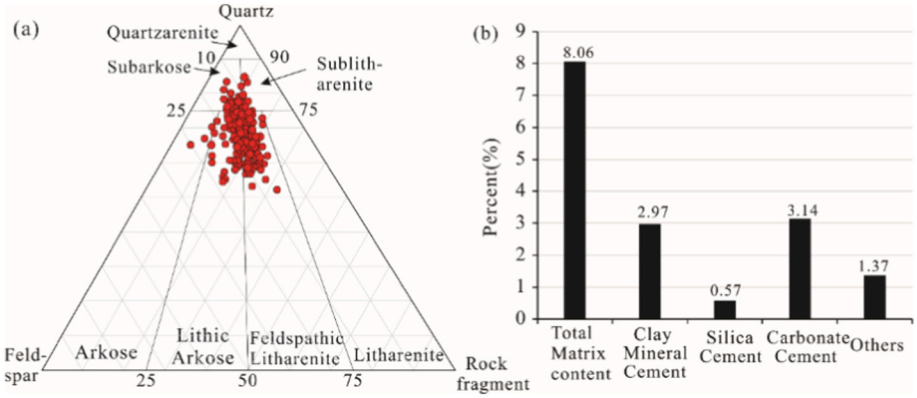

Fig. 3. (a) Triangular diagram of compositional components (Folk, 1980); (b) Matrix characteristics of E_3h sandstones.

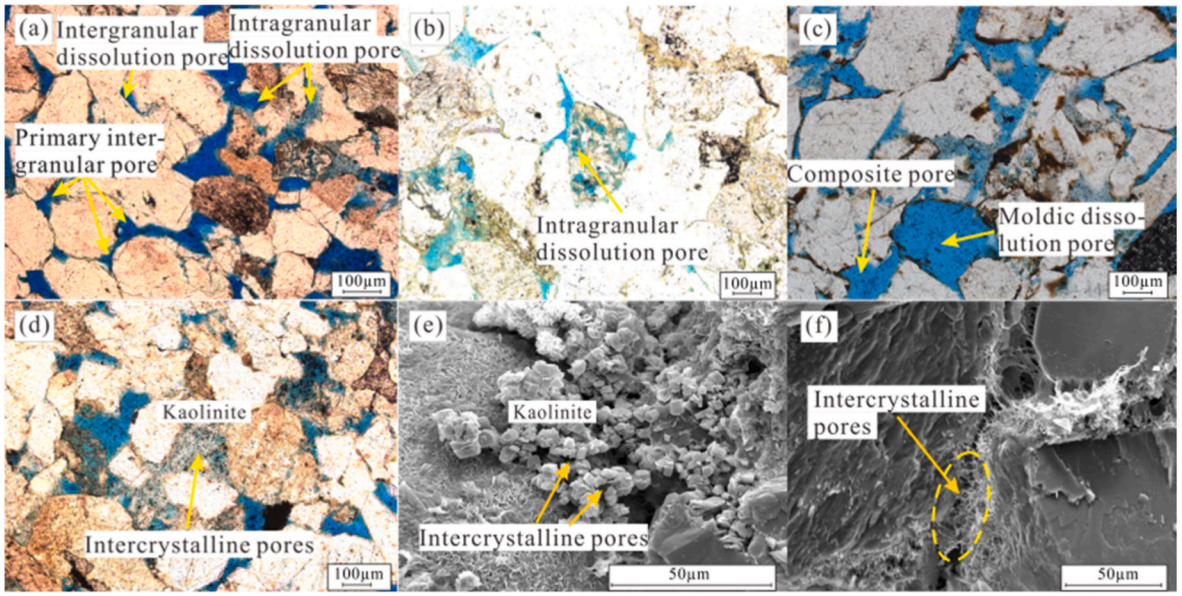

Fig. 4. Pore characteristics of E_3h reservoirs in the study area. (a) Residual intergranular pores developed, 3872.7 m, Well A-3; (b) Intragranular dissolution pores, 3963.4 m, Well A-2; (c) Moldic dissolution pores, 3533.5 m, Well A-1; (d) Intercrystalline pores in kaolinite, 3868.72 m, Well A-3; (e) Chlorite and kaolinite filling pores (SEM image), 4187 m, Well B-3; (f) Filamentous illite filling intergranular pores (SEM image), 3659 m, Well B-3.

extreme compaction, phenomena such as fractured quartz grains and curved/deformed plastic grains (e.g., rock fragments, mica) are observed (Fig. 5a and b). These observations support the interpretation that mechanical compaction significantly influences sandstone quality.

4.3.2. Cementation

Cementation is a crucial factor in reducing reservoir porosity. Analytical results show that authigenic cements in E_3h reservoirs are categorized into three types: clay cements, carbonate cements, and siliceous cements.

4.3.2.1. Clay cement. XRD analysis indicates that clay minerals in E_3h reservoirs are dominated by illite-smectite mixed layers (I/S, with an average content of 4.04 %) and illite (I, avg. 3.95 %), followed by chlorite (Ch, avg. 1.61 %) and kaolinite (K, avg. 1.00 %). Kaolinite content decreases rapidly with depth: in shallow reservoirs (<3600 m), kaolinite dominates and fills intergranular pores, coexisting with dissolution pores (Fig. 6g); in deeper reservoirs (>3600 m), kaolinite content declines and only occasionally fills pores. With increasing burial depth, the contents of illite and illite-smectite (I/S) mixed layers exhibit a consistent upward trend. In reservoirs deeper than 3600 m, the elevated illite content stems from dual sources: the transformation of kaolinite and I/S minerals, as well as direct precipitation from pore fluids. Illite predominantly occurs as hairy or filamentous aggregates, filling intergranular pores and altering the reservoir's pore structure.

Chlorite content demonstrates a depth-dependent pattern of initial increase followed by decrease. As burial depth progresses from 3300 m to 4000 m, chlorite content reaches a peak of up to 8 % (Fig. 6d), accompanied by the development of well-crystallized grain-coating and pore-lining chlorite (Fig. 6h). This chlorite coating effectively resists compaction and preserves primary pores. However, further burial leads to a decline in chlorite content, with the remaining chlorite displaying uneven distribution in basal HG Formation reservoirs. Here, it is predominantly present as flaky or rosette-shaped aggregates, with an overall content of approximately 1.5 %.

4.3.2.2. Carbonate cement. Carbonate cements represent typical diagenetic phases in the study area, dominated by calcite (Fig. 7a–c) with subordinate dolomite, fe-calcite, and ankerite (Fig. 7d–f). Two distinct cementation stages are identified: Early calcite cements, formed during shallow burial, preferentially fill primary intergranular pores and develop as basal coatings adjacent to mudstone interlayers, resulting in detrital grains floating within the carbonate matrix with point or no physical contacts (Fig. 7a and b). Late fe-carbonate cements, the

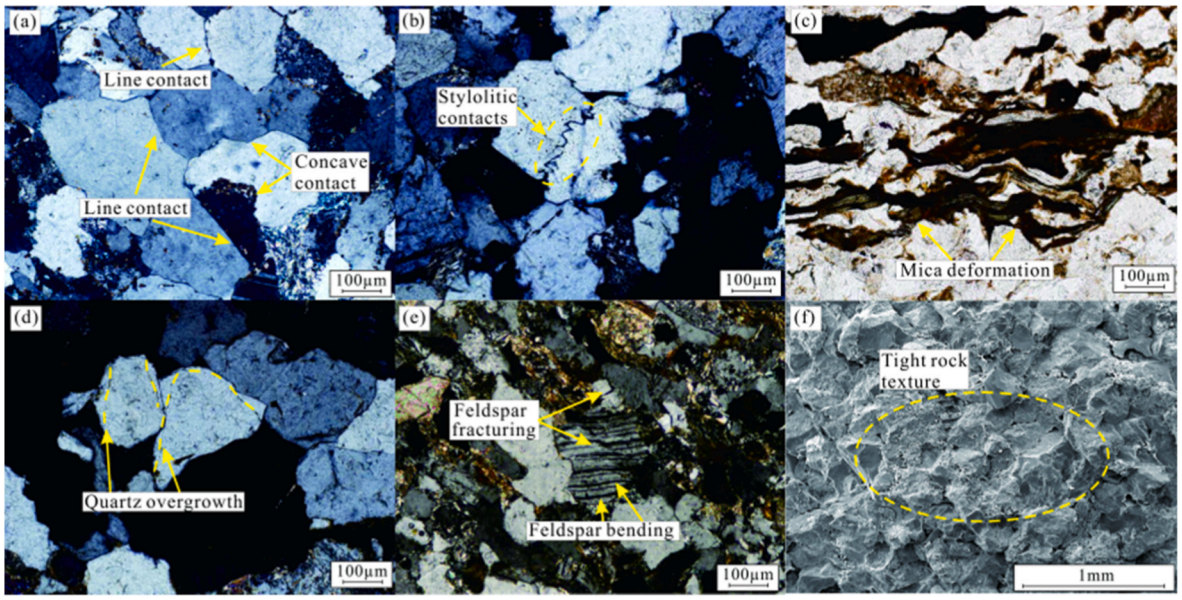

Fig. 5. Micrographs show compaction characteristics of E_3h sandstones. (a) Line-concave contacts, 4186.01 m, Well B-3; (b) Stylolitic contacts, 3422 m, Well B-2; (c) Mica deformation, 3938 m, Well B-1; (d) Quartz overgrowth, 3428 m, Well B-2; (e) Feldspar bending and fracturing, 4187 m, Well A-2; (f) Tight rock texture, 4181.5 m, Well A-2.

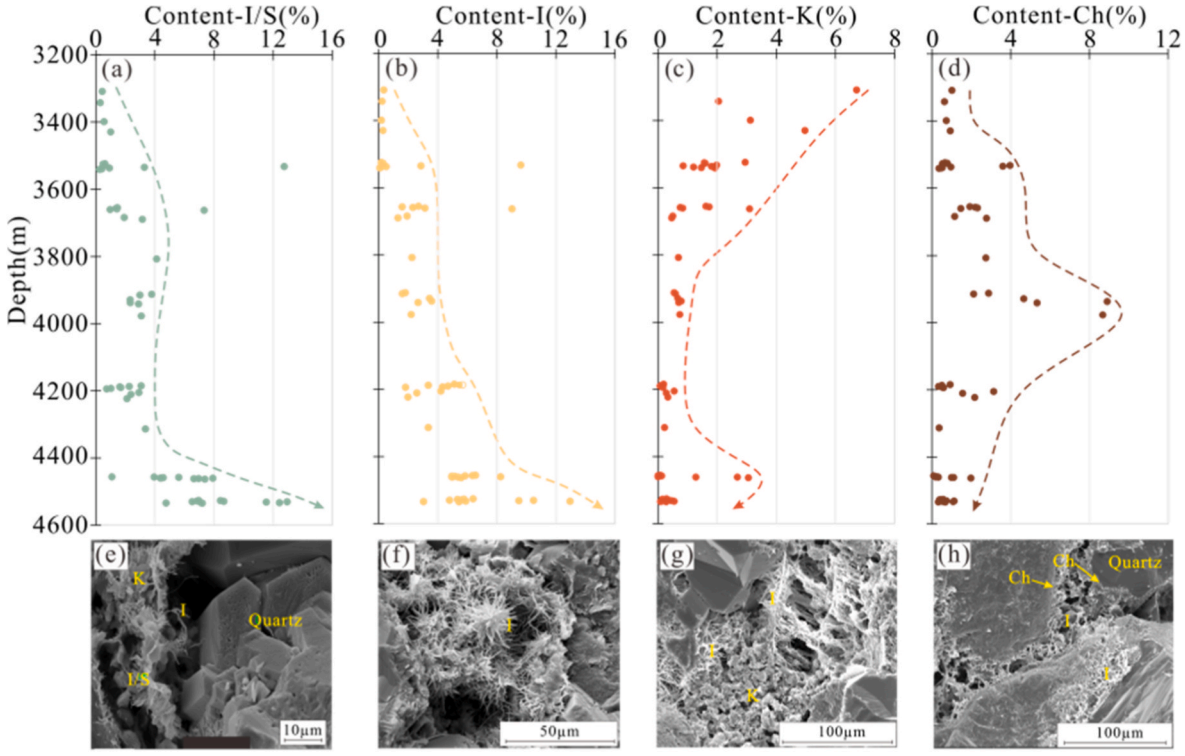

Fig. 6. Contents of illite-smectite mixed layers (a), illite (b), kaolinite (c), and chlorite (d) and their variations with depth. (e) Laminated kaolinite coexisting with I and curly flaky I/S, 3873.12 m, Well A-3. (f) Hairy and curly illite aggregates, 4187 m, Well A-2; (g) Feldspar dissolution associated with authigenic kaolinite, 3428 m, Well B-2. (h) Grain-coating chlorite, 3937 m, Well B-1.

principal diagenetic minerals inducing reservoir quality degradation, exhibit deep purple to dark red hues under staining. These cements replace preexisting minerals or occlude pore throats along margins, thereby exacerbating porosity loss (Fig. 7d–f).

4.3.2.3. Siliceous cement. Quartz overgrowths occur along framework quartz grain margins (Fig. 5d), exhibiting euhedral crystal morphology (Fig. 6e). Quartz cement content ranges from 0 to 7.2 % (average 1.2 %) and is absent in chlorite-coated areas (Fig. 6h), with overgrowths terminating at grain contacts.

4.3.3. Dissolution

Dissolution is a critical constructive diagenesis commonly observed in reservoirs, contributing to pore development and the formation of

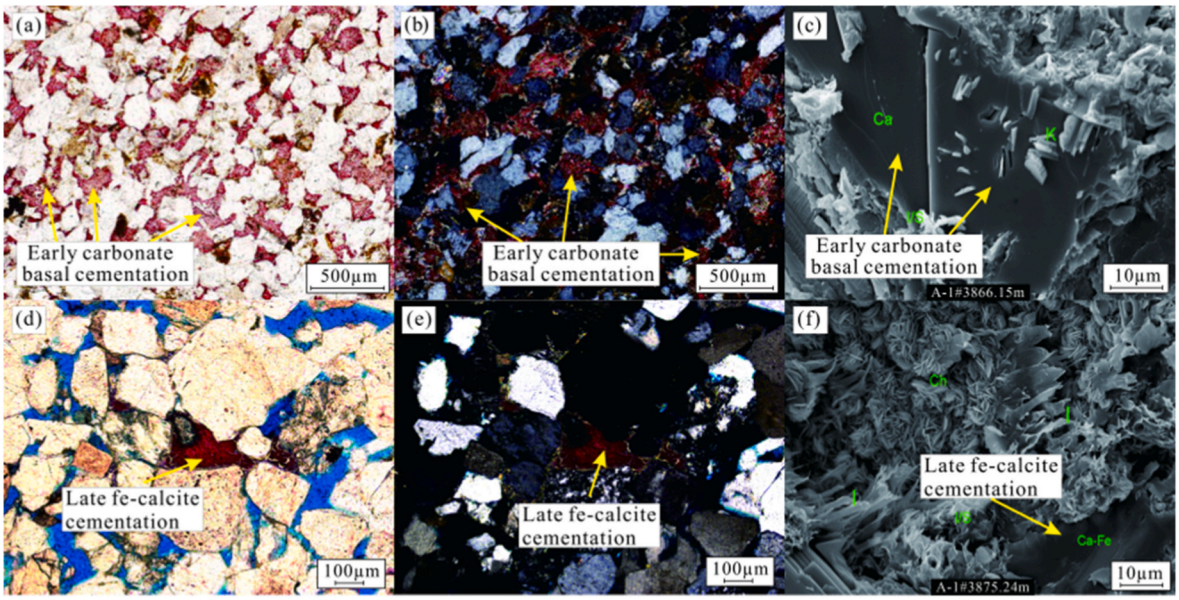

Fig. 7. Microscopic characteristics of carbonate cements. (a) Early carbonate basal cementation, 3937.1 m (−), Well B-1; (−) denotes plane-polarized light (single polarizer). (b) Early carbonate basal cementation, 3937.1 m (+), Well B-1; (+) denotes cross-polarized light (orthogonal polarizers). (c) Early carbonate basal cementation, 3866.15 m (SEM), Well A-3; (d) Late fe-calcite cementation, 3874.2 m (−), Well A-3; (e) Late fe-calcite cementation, 3874.2 m (−), Well A-3; (f) Late ankerite cementation, 3875.2 m (SEM), Well A-3.

high-quality reservoirs. Secondary dissolution pores in E_3h sandstones generally account for more than 50 % of the total pore area. Unstable components such as feldspar and lithic fragments are the main contributors to dissolution pores, with some argillaceous matrix also dissolved to form secondary pores. Microscopically, abundant intergranular and intragranular dissolution pores are observed (Fig. 4a–c), and moldic pores may form under intense dissolution (Fig. 4c). Intergranular dissolution pores generated by dissolution are the dominant pore type in the study area, primarily forming along the margins or within feldspar grains (Fig. 4c). Rock fragment dissolution is also visible in the reservoirs (Fig. 4b), with occasional carbonate cement dissolution.

4.4. Porosity and permeability

Core analysis results show that porosity ranges from 2 % to 15.8 % (average 9.07 %), while permeability varies between 0.01 and 100 mD (average 1.41 mD) (Fig. 8). A strong positive correlation exists between porosity and permeability; however, individual samples with developed fractures exhibit anomalously high permeability (Fig. 8b–c). Petrophysical properties vary with depth (Fig. 8d–e). Shallow sandstones display higher porosity, peaking at 18 % around 3300 m depth, but rapidly decline to ~13 % at 4200 m. Without considering fractures, permeability trends similarly to porosity, decreasing with depth. However, due to diagenetic modification and fracture development, the maximum permeability occurs at ~3500 m depth.

Based on core analysis, logging data (lithology, porosity, permeability), and drill-stem results (DST), and referring to the reservoir evaluation criteria from the Shanghai Branch of CNOOC (China) Ltd., reservoirs with porosity >9 % and permeability >0.2 mD are defined as effective reservoirs (Yang, 2023), while those below this threshold are ineffective reservoirs. Both reservoir types are distributed across varying

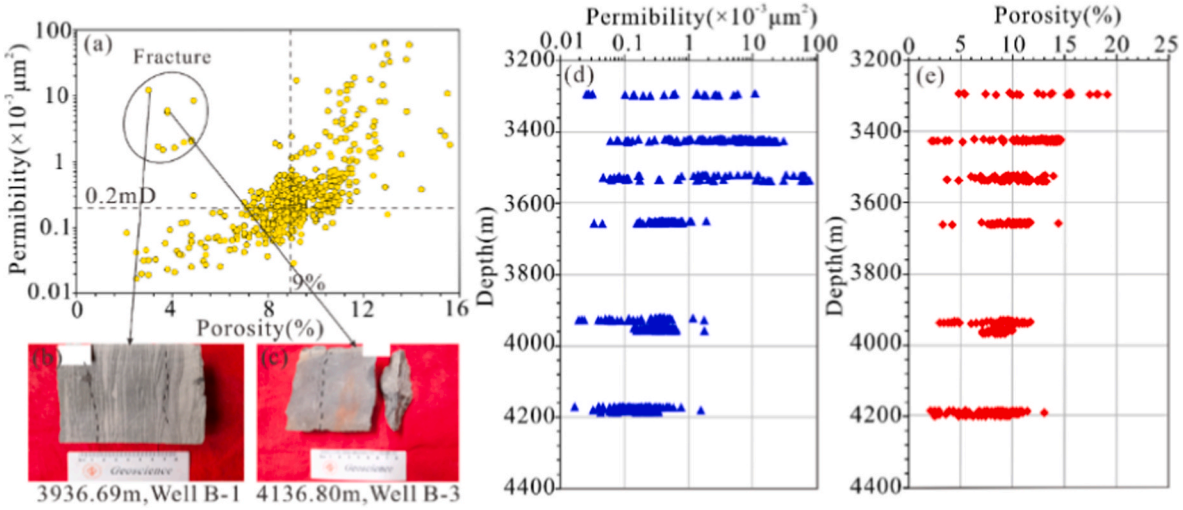

Fig. 8. (a) Crossplot of porosity vs. permeability for E_3h sandstones. Photographs showing fracture development characteristics in core samples from Well B-1 at 3936.69 m (b) and Well B-3 at 4136.80 m (c), respectively. Variation trends of permeability (d), porosity (e) with depth.

depths. Significant differences in diagenetic processes exist between the two reservoir types: effective reservoirs are characterized by intense dissolution, while ineffective reservoirs exhibit strong cementation and compaction. High-pressure mercury injection results show that effective reservoirs have porosity ranging from 9.31 % to 14.51 % and abundant microscale pores (Fig. 9). In contrast, ineffective reservoirs have poor petrophysical properties (low porosity and permeability) dominated by nanoscale and sub-microscale pores, indicating they are ineffective/low-quality reservoirs.

4.5. Burial history

Results indicate that the E_3h experienced three tectonic movements: the Huagang Movement at the end of the Oligocene, the Longjing Movement at the end of the Miocene, and the Okinawa Movement at the end of the Pliocene (Liu et al., 2020; Zhou et al., 2020; Zou et al., 2021). The Longjing Movement subjected the strata to intense compression, uplift, and erosion, exerting significant influence on the physical property evolution of E_3h reservoirs (Zou et al., 2021). Combining stratigraphic subsidence rates, tectonic activities, and published literature, the burial history of E_3h reservoirs is divided into three periods.

Gradual subsidence stage (GSS): early Oligocene to the end of N_1^1l (32–13 Ma). The E_3h sandstone began depositing with increasing burial depth. The Huagang Movement occurred at 23.3 Ma but had minimal impact on reservoir modification. Tectonic activity stage (TAS): End of N_1^1l to mid-N_1^2y (13-8 Ma). During the early period of this stage, the burial depth of the E_3h rapidly increased, with the deepest layer in the Well block A reaching about 4000 m. At ~11.0 Ma, the E_3h in the study area was significantly uplifted and severely eroded, with erosion thickness ranging from 50 to 200 m. Stable burial stage (SBS) (8 Ma to present): During N_1^3l, N_{2st} and Qd strata deposition, E_3h experienced stable subsidence. The Okinawa Trough Movement had a negligible impact on the study area (Fig. 10a).

4.6. Fluid inclusions analysis

Based on collected data, fluid inclusions in sandstone samples are primarily distributed in quartz overgrowth rims and microfractures cutting through quartz, with shapes including spherical, ellipsoidal, and irregular forms. Sizes range from 1 to 7 μm, and inclusions occur in either gas-liquid two-phase or liquid phases.

Homogenization temperatures of fluid inclusions in quartz overgrowth rims and authigenic quartz were measured, as shown in Fig. 11. Inclusions in the first-stage quartz overgrowth exhibit temperatures ranging from 104 to 120 °C (average 113.46 °C), while those in the second-stage overgrowth yield temperatures of 137.62 °C (121–155.6 °C).

4.7. Carbon and oxygen isotopes of carbonate cements

Carbon and oxygen isotope results of carbonate cements from 14 sandstone samples (Table 2) show that $\delta^{13}C$ values in the study area range from −3.7 ‰ to 0.25 ‰, while $\delta^{18}O$ values range from −10.3 ‰ to −19.73 ‰. Isotopic compositions differ between carbonate cements formed at different stages. For first-stage calcite cements, $\delta^{13}C$ ranges from −3.7 ‰ to 0.25 ‰ and $\delta^{18}O$ ranges from −10.3 ‰ to −19.73 ‰. For second-stage calcite cements, $\delta^{13}C$ also ranges from −3.7 ‰ to 0.25 ‰ and $\delta^{18}O$ from −10.3 ‰ to −19.73 ‰. Empirical formulas proposed by Keith and Weber were applied to calculate the paleosalinity Z value (Keith and Weber, 1964), and formation temperatures of carbonate cements were calculated using Shackleton's empirical formula (Shackleton, 1987).

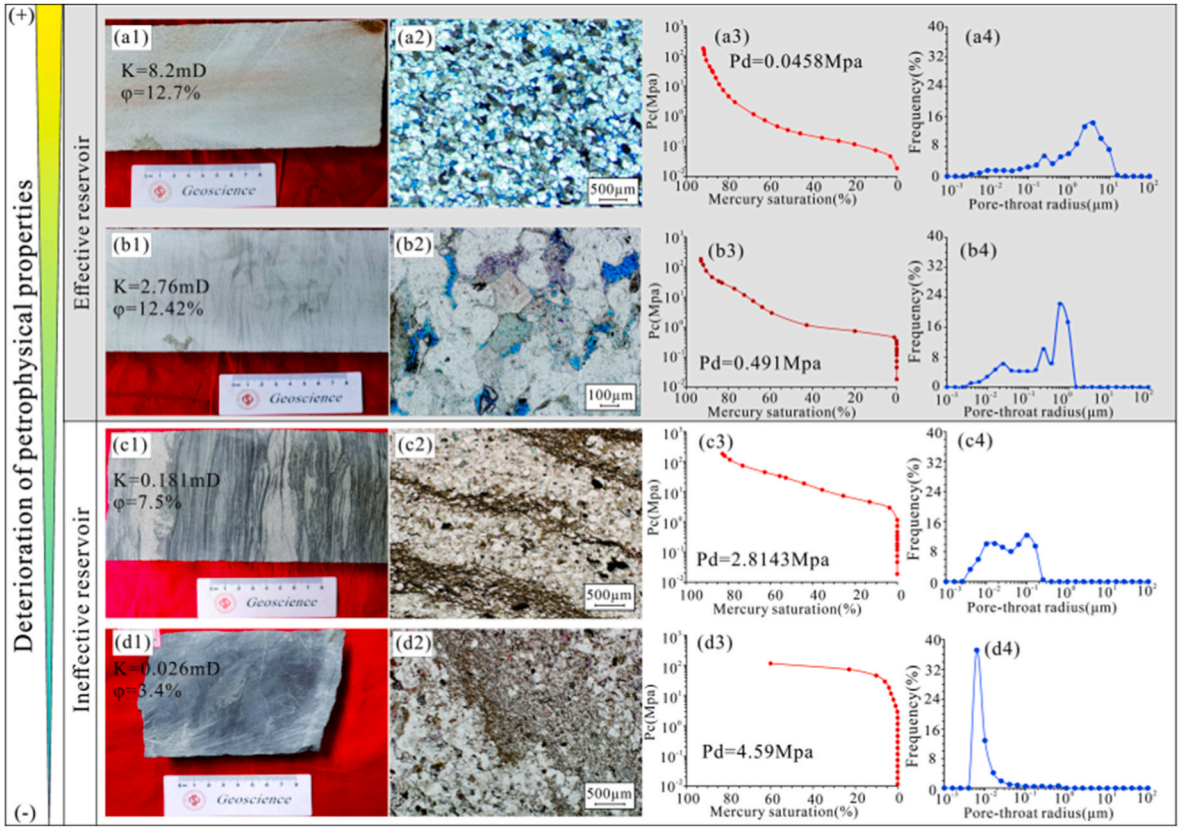

Fig. 9. Petrophysical properties and pore distribution characteristics of different reservoir types. Effective reservoirs at 3863.72 m (Well A-3), showing micro-scale pore dominance (a1-a4). Effective reservoirs at 3428.3 m (Well B-2), showing submicro-scale pore dominance (b1-b4). Ineffective reservoirs at 3293.16 m (Well B-1), showing submicro to nano-scale pore dominance (c1-c4). Ineffective reservoirs at 4192.63 m (Well B-3), showing nano-scale pore dominance (d1-d4).

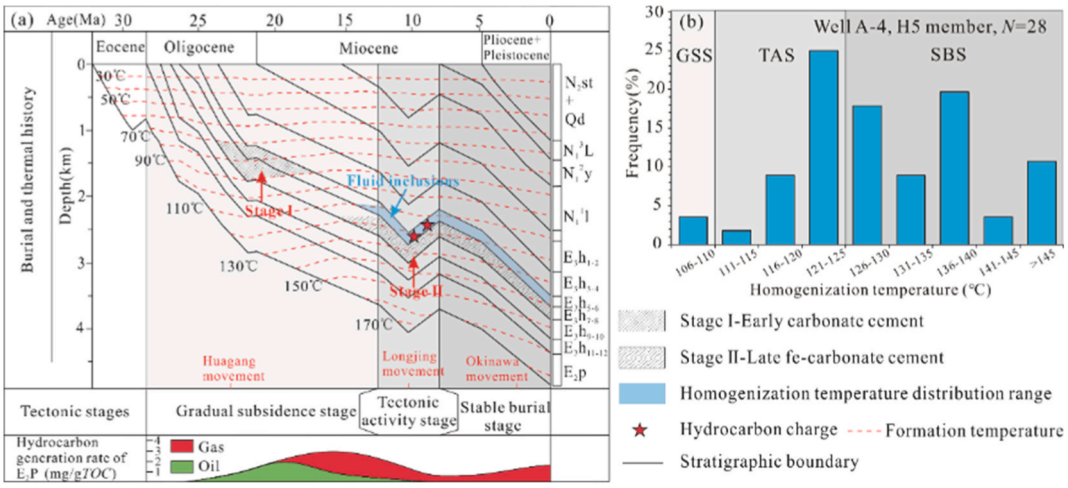

Fig. 10. (a) Burial history, tectonic stage division of Well A-4, and formation timing of carbonate and quartz cements in sandstone reservoirs. (b) Histogram of homogenization temperatures for fluid inclusions in H5 member sandstone samples from Well A-4.

5. Discussion

5.1. Diagenetic stages and evolutionary sequence

5.1.1. Diagenetic stage

Based on previous studies and physical-chemical indicators such as authigenic clay mineral assemblages, the diagenetic stages of the study area were classified using the Classification Scheme for Diagenetic Stages of Clastic Rocks (SY/T 5477-2003) issued by CNPC in 2003, following the main criteria for clastic rocks in freshwater-brackish water environments.

The E_3h sandstone reservoirs in the study area are buried at 3200–4400 m depth, characterized by moderate-deep burial and intense compaction. Detrital grains exhibit dominantly point-line contacts, with rare concavo-convex contacts (Fig. 5). Two stages of quartz overgrowth are observed, with formation temperatures ranging from 104 to 155.6 °C (Fig. 11). Early carbonate cements occur as basal cementation, while late fe-carbonates fill pores in powdery crystalline form (Fig. 7). Additionally, smectite content in I/S mixed layers ranges from 15 % to 30 %. Clay minerals are dominated by kaolinite, I/S mixed layers, illite, and chlorite, free of smectite. These mineralogical compositions, pore types, clay mineral transformations, and paleotemperatures suggest that the reservoir diagenesis is primarily at stage A of the mesogenetic phase.

5.1.2. Diagenetic evolutionary sequence

Establishing a diagenetic evolutionary sequence requires not only classifying diagenetic stages but also determining the reservoir's diagenetic paragenetic sequence to clarify the temporal order of diagenetic processes and cement development.

Silica sources of E_3h sandstones in the study area include four aspects: feldspar dissolution, lithic fragment dissolution, clay mineral transformation, and quartz grain dissolution (Hyodo et al., 2014; Peng et al., 2020; Lin et al., 2024). The formation of saline inclusions corresponds to optimal physico-chemical conditions for authigenic quartz growth (Lander et al., 2008; Lander and Laubach, 2015). Homogenization temperatures of saline inclusions in quartz overgrowths are 104°C–120 °C and 121°C–155 °C (Fig. 11). Projecting these homogenization temperatures onto the burial thermal history plot reveals that quartz cementation occurred between 14.5 Ma and 0.0 Ma.

Relatively low negative $\delta^{13}C$ values indicate that decarboxylation reactions of organic matter in adjacent mudstones and source rocks are significant carbon sources for E_3h sandstone (Table 2) (Irwin et al., 1977; Wang et al., 2020). Calculated precipitation temperatures of carbonate cements show that first-stage calcite cements formed at 70°C–90 °C, while late fe-carbonate cements precipitated at ~115°C–143 °C (Table 2). During E_3h sandstone deposition, the sedimentary environment was freshwater-brackish. The formation of late fe-carbonate cements indicates an acidic diagenetic environment. Combined with burial and thermal history, early calcite cements precipitated from syngenetic alkaline pore fluids in the late Oligocene. Formation of late fe-carbonate cements began in the mid-Miocene and continues to the present, consistent with previous studies (Qian et al., 2020; Wang et al., 2020; Zhou et al., 2020).

Based on these findings, the formation of early calcite cements preceded siliceous cements, while fe-carbonate cements formed later than quartz overgrowth cements. During deposition, compaction proceeded continuously, with increasing intensity as burial depth increased. Following the dissolution of feldspar and other minerals by organic acid influx into sandstones, later-stage quartz overgrowth rims formed, and dissolution pores along feldspar joints or moldic pores provided effective hydrocarbon accumulation spaces. This reflects a transition in the diagenetic environment from weakly alkaline to weakly acidic. Therefore, the diagenetic evolutionary sequence of the target interval is: Early weak compaction of rock grains→ Meteoric water dissolution of feldspar and lithic fragment→ Early calcite cementation→ Intense compaction and early quartz overgrowth→ Large-scale dissolution of feldspar, carbonate cements, and lithic fragments→ Late-stage quartz overgrowth→ Late fe-carbonate cementation→ Clay mineral transformation (Fig. 12).

5.2. Diagenetic controls on reservoir quality

5.2.1. The effect of compaction on reservoir quality

Reservoir quality of E_3h sandstone is significantly influenced by diagenetic processes and products, with mechanical compaction being the primary cause of substantial quality degradation. A crossplot of porosity loss due to compaction versus cementation (Fig. 13a) indicates that compaction-induced porosity reduction is dominant (Ehrenberg, 1989). Additionally, Fig. 13a shows that most samples have primary intergranular porosity <20 %, confirming compaction (not cementation) as the main factor for reduced intergranular porosity (Houseknecht, 1987; Ehrenberg, 1989). On average, Fig. 13a suggests that samples lost >50 % of their initial porosity due to mechanical compaction. Furthermore, residual intergranular pores-depth correlation plots (Fig. 13b) reveal rapid declines in reservoir porosity and permeability with increasing burial depth, as well as decreasing residual intergranular pores, indicating stronger compaction in deeper sandstone reservoirs.

Compaction is influenced by grain size and sorting, which are closely

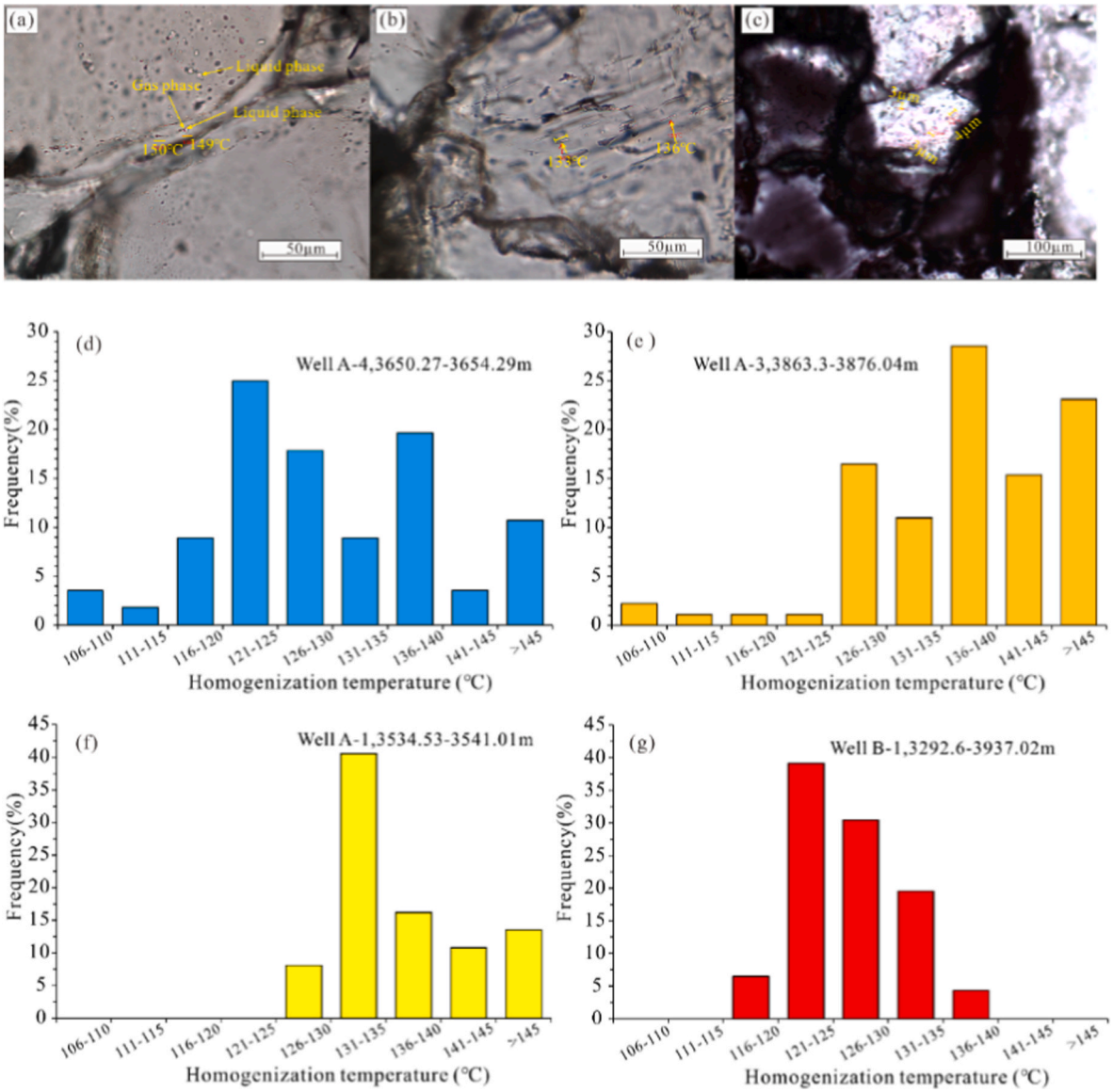

Fig. 11. Fluid inclusion types and homogenization temperatures in E_3h reservoirs. (a) Inclusions distributed along quartz overgrowth rims, 3876.04 m, well A-3; (b) Gas-liquid two-phase inclusions in healed microfractures cutting quartz grains, 3876.04 m, well A-3; (c) Liquid-rich and gas-liquid two-phase inclusions, 3295 m, well B-1; (d–g) Histogram of homogenization temperatures of aqueous fluid inclusions in quartz overgrowths from E_3h sandstones, Wells A-4, A-3, A-1, and B-1.

Table 2
Distribution characteristics of isotopes in sandstone carbonate cements.

Well	Depth (m)	Member	$\delta^{13}C$ (‰,VPDB)	$\delta^{18}O$ (‰,VPDB)	Mineral	Type	Z value	Temperature (°C)
A-2	3958.3	H8	−3.26	−19.73	Fe-calcite	Late	110.8	142.2
A-2	3960.2	H8	−0.16	−16.78	Fe-calcite	Late	118.6	118.5
A-2	3963.6	H8	−4.09	−18.75	Fe-calcite	Late	109.6	134.1
A-2	3965.6	H8	−3.7	−17.28	Fe-calcite	Late	111.1	122.4
A-2	3966.2	H8	−3.48	−16.33	Fe-calcite	Late	112.0	115.1
A-2	3967.2	H8	−0.53	−19.1	Fe-calcite	Late	116.7	137
A-4	3647.3	H5	0.01	−11.01	Calcite	Early	121.8	77.2
A-4	3648.7	H5	0.25	−10.3	Calcite	Early	122.6	72
A-4	3650.9	H5	−3.07	−12.67	Dolomite	Early	114.7	88.4
A-4	3651.3	H5	−3.08	−12.58	Calcite	Early	114.7	87.8
A-4	3653.7	H5	−2.54	−18.12	Fe-calcite	Late	113.1	129.1
A-4	3655.1	H5	−1.22	−19.06	Fe-calcite	Late	115.3	136.7

related to sedimentary microfacies (Baiyegunhi et al; Zhang et al., 2022). The study area is predominantly characterized by braided river and delta sediments (Min et al., 2023). In thick sandstones, such as those found in channel bars and main channels, fine-grained sandstones with good sorting typically exhibit point contacts between grains, well-developed primary pores, and low plastic matrix content. This combination results in weaker compaction during subsequent burial. In contrast, sandstones located between distributary channels tend to have

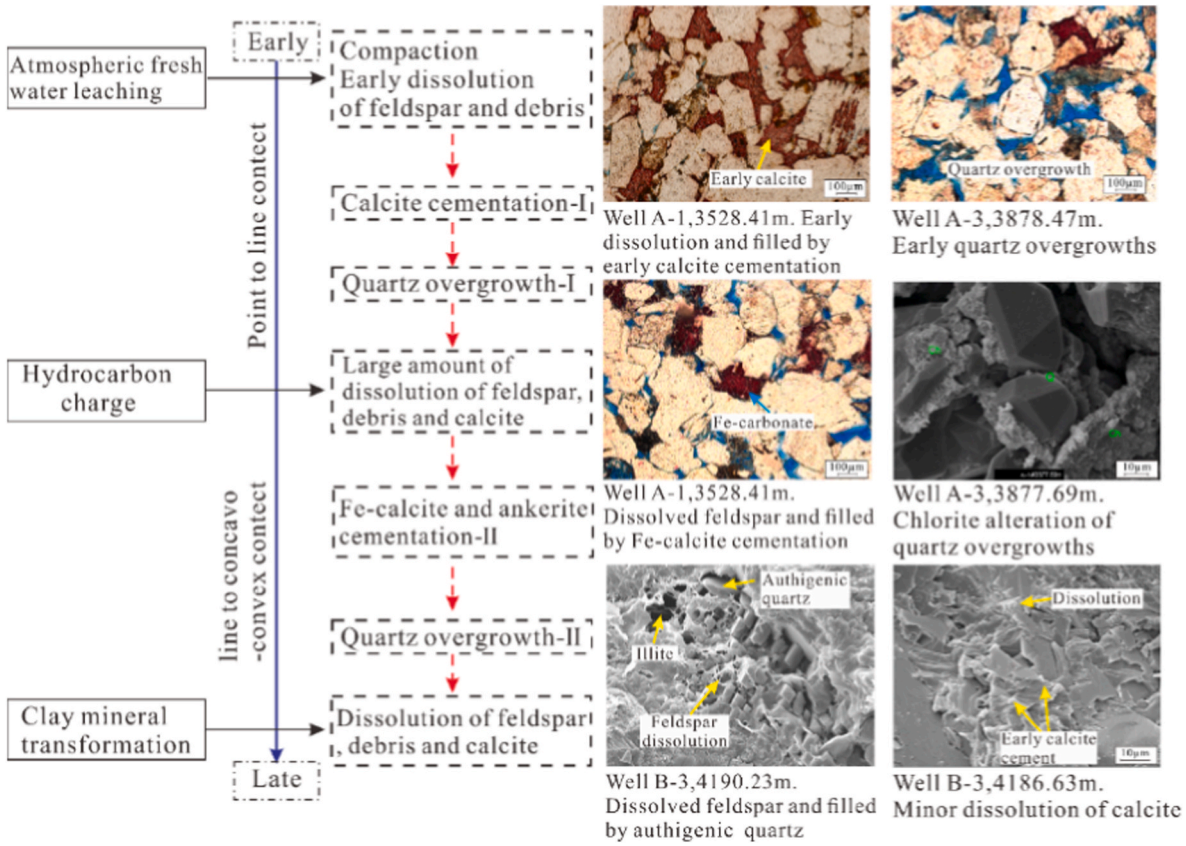

Fig. 12. Diagenetic evolutionary sequence of E_3h reservoirs in the study Area.

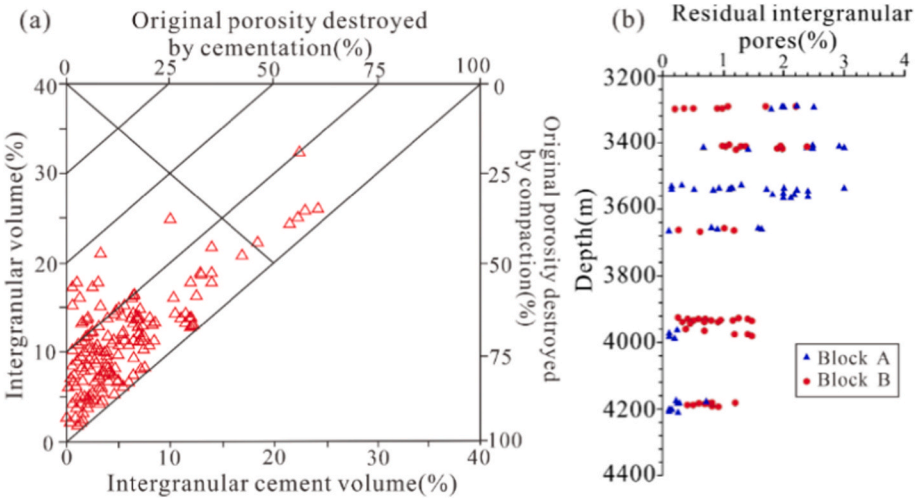

Fig. 13. (a) Crossplot of intergranular volume (IGV) vs. intergranular cement volume (ICV) of E_3h sandstones (Ehrenberg, 1989); (b) Variation of residual intergranular pore content with depth of E_3h sandstones.

fine grain sizes, poor sorting, high matrix content, and limited primary pores. The plastic nature of the matrix contributes to significant compaction during burial, which further reduces porosity and permeability. On the other hand, coarser-grained reservoir rocks are more resistant to overburden compaction, allowing them to preserve primary pores. This preservation facilitates pore fluid flow and enhances late-stage secondary dissolution, ultimately improving reservoir quality. For example, Well A-3 (3863.72 m) contains delta front underwater distributary channel fine sandstones with highly developed pores (Fig. 9a1-a4). In contrast, Well B-1 (3293.16 m) consists of argillaceous siltstones located between delta front distributary channels, which have poorly developed pores (Fig. 9c1-c4).

5.2.2. *Impact of cementation on reservoir quality*

In addition to compaction, cementation plays a crucial role in reducing reservoir quality. In various diagenetic environments, the accumulation of authigenic minerals as dispersed pore-filling cement can locally decrease the effective intergranular pore volume. This alteration impacts the reservoir storage capacity and flow paths of E_3h sandstones, ultimately degrading the reservoir quality.

Carbonate cements are frequently found in E_3h reservoirs, with concentrations varying between 1 % and 33 %. When the cement content is less than 5 %, there is a weak negative correlation between reservoir porosity and permeability with calcite content. However, when the cement content exceeds 5 %, the correlation with calcite content becomes stronger, though with a low slope (Fig. 14). This indicates that at cement contents below 5 %, the decline in porosity and permeability is primarily driven by compaction, while carbonate cementation has a limited impact on reservoir properties. When calcite content exceeds 5 %, the increasing cementation begins to significantly occlude pore space and block pore throats. Consequently, this more profound reduction in primary porosity leads to calcite cementation becoming the main factor degrading reservoir physical properties at higher cement contents.

At the interface between sand and mud, the compaction process causes pore water to be expelled from mudstones, leading to the formation of carbonate-cemented zones at both the top and bottom of sandstones. This process makes the sandstones nearly impermeable. Early carbonate minerals can replace framework grains such as quartz and feldspar. Possible sources for late authigenic calcite include the dissolution of early carbonates, the dissolution of plagioclase, and the illitization of smectite. For example, in Well B-3, H11 member, at a depth of 4193.85 m, sample (d) (which is a coarse to medium-grained feldspathic litharenite) was collected from the base of the sand body. Microscopic observations reveal significant replacement of detrital grains by late calcite cements. The sample shows basal cementation, with grains exhibiting point or no contacts (floating), and the content of carbonate cement exceeds 15 % (Fig. 15).

Clay mineral cements are common in E_3h sandstones of the study area, obstructing reservoir storage capacity and flow pathways through pore filling and throat plugging, thus significantly harming reservoir quality. Different types of clay minerals have varying effects on reservoir quality.

The distribution of illite and illite-smectite mixed layers varies with the depth of the reservoir. Higher concentrations of these clay minerals lead to a rapid decrease in dominant pore throat radii, an increase in tortuosity, and an exponential decline in permeability (Fig. 16d). Kaolinite is widely found throughout the study area. In reservoirs deeper than 3700 m, kaolinite appears as vermicular aggregates that fill residual primary intergranular pores and intergranular dissolution pores. The formation of kaolinite is indicative of significant development of dissolution porosity, which generally enhances reservoir quality as the kaolinite content increases (see Fig. 16e and f). However, the limited expulsion of feldspar dissolution products can lead to kaolinite aggregates that completely occlude pores, thereby constraining the potential improvement in reservoir quality.

Early chlorite coatings on E_3h reservoir grains provide significant resistance to compaction (Zhang et al., 2022). Quartz and feldspar grains that are encapsulated by chlorite films exhibit minimal deformation or fracturing, which locally enhances the quality of the reservoir. However, during early diagenesis, sediments transported in high-energy hydrodynamic environments led to the adsorption of most dissolved Fe-Mg ions onto grain surfaces as flocculated colloids. By the time these sediments reached the study area, the concentration of Fe-Mg ions had significantly decreased. As a result, the clay coatings on grain surfaces did not transform into chlorite films during the later stages, leading to the predominance of pore-filling chlorite in E_3h reservoirs. This mineralogical configuration negatively impacts reservoir quality by reducing pore connectivity and permeability (Fig. 16g and h).

5.2.3. *The effect of dissolution on reservoir quality*

Leaching caused by meteoric freshwater and organic acids produced from the thermal evolution of E_2p mudstones has dissolved soluble minerals such as feldspar, clastics, and early calcite cements. This process has promoted the formation of secondary porosity zones. The intensity of leaching significantly affects the development of secondary pores (Zhang et al., 2022). Generally, a higher intensity of dissolution leads to improved petrophysical properties of the reservoir (Wang et al., 2019).

Secondary dissolution pores are an important type of pore in the E_3h reservoirs of the study area. The dissolution process has enhanced the quality of sandstone reservoirs. Calculations from cast thin sections indicate that dissolution has led to increases in porosity ranging from 0.5 % to 6.5 %, with an average increase of 3.6 %. Notably, there are differences in dissolution-induced porosity between different blocks, with Block A showing an average increase of 3.7 % and Block B showing an average increase of 3.5 %. As shown in Fig. 8d, significant property improvements in E_3h reservoirs occur at depth intervals of 3420–3440 m and 3520–3540 m, which correspond to the secondary porosity zones illustrated in Fig. 18c. Although the dissolution of chemically unstable feldspar and mica grains has resulted in the formation of grain-replacing kaolinite, this process generally contributes to an increase in total porosity in sandstones.

5.3. *Factors controlling effective reservoirs and formation mechanisms*

5.3.1. *Coupling of diagenesis and burial history determines effective reservoir formation potential*

During the gradual subsidence stage (GSS), E_3h reservoirs were primarily composed of deltaic medium to fine-grained sandstones, establishing favorable material and initial conditions for effective reservoir formation. At this stage, E_3h sandstone reservoirs were submerged in

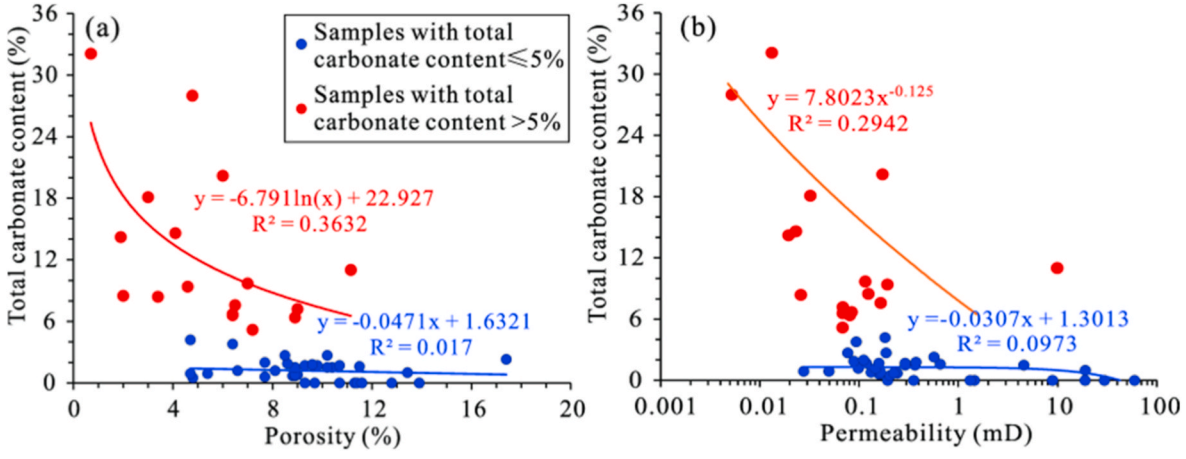

Fig. 14. Crossplot of carbonate cement content vs. porosity (a) and permeability (b) of E_3h sandstones.

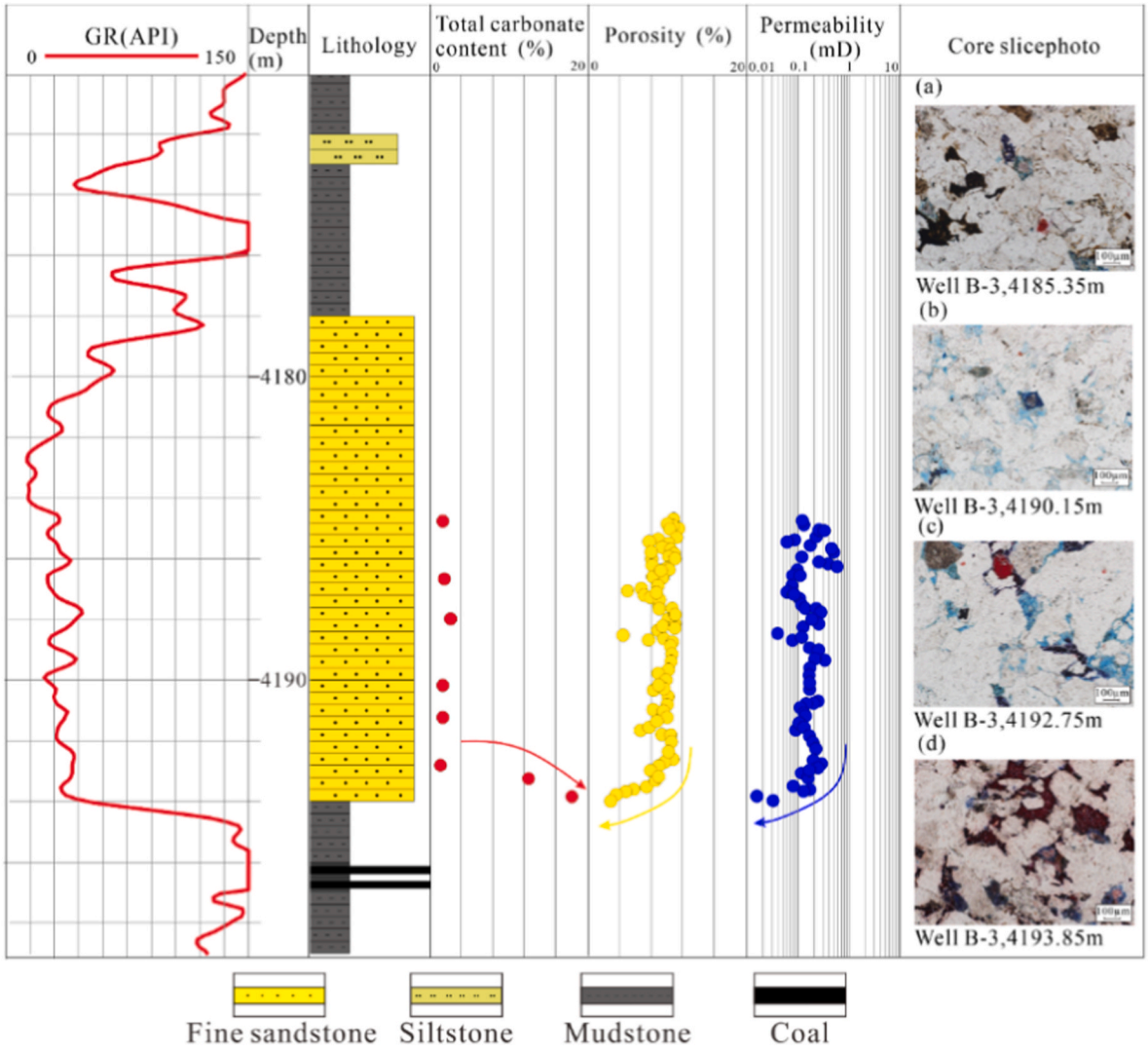

Fig. 15. Relationship between carbonate cement content and petrophysical parameters in H11 Member sandstones of Well B-3.

syngenetic alkaline pore water, conducive to chlorite coating and early calcite cement formation. Diagenetic processes, including compaction, early calcite cementation, and chlorite coating development, caused significant reductions in sandstone porosity and permeability. The late Oligocene Huagang Movement induced strata uplift and erosion. Accompanied by meteoric water invasion, sandstone reservoirs experienced a weakly acidic diagenetic environment, where dissolution of feldspar, lithic fragments, and calcite cements formed feldspar dissolution pores and intergranular dissolution pores (Yang et al., 2024). This enhanced sandstone porosity and permeability.

During the tectonic activity stage (TAS), E_3h sandstone reservoirs in the study area experienced rapid burial, leading to rapid temperature increases. Maximum temperatures reached 130 °C in Well A-2's H5-H6 Member (western area) and 120 °C in the eastern Well B-2. While in the late TAS, strata uplift-erosion occurred, reducing reservoir temperatures (Fig. 17) and enabling authigenic quartz precipitation at low temperatures. Anticlinal structures were finally established during this period. Additionally, fault activation during tectonic activity allowed hydrocarbons generated from E_2p source rocks to enter reservoirs. These organic acids reacted with feldspar, lithic fragments, and carbonate cements in E_3h sandstones, forming secondary pores, quartz cements, and authigenic kaolinite, thereby increasing reservoir pore space. Optimal temperatures for organic acid preservation (80–120 °C) triggered decarboxylation of organic acids into hydrocarbons and CO_2 (Fig. 17) (Wang et al., 2021). Concomitant with declining organic acid concentrations, massive CO_2 generation favored iron-bearing calcite cementation (Chen et al., 2024; Huang et al., 2020).

During the stable burial stage (SBS), following the termination of the Longjing Movement, continued burial of sandstone reservoirs led to peak temperatures in the evolution history (Fig. 17). At this stage, late-stage calcium-iron minerals, illite, and chlorite formed in E_3h sandstone reservoirs. With increasing depth and temperature, enhanced feldspar dissolution and clay mineral transformations provided abundant SiO_2 sources for authigenic quartz precipitation in adjacent acidic diagenetic environments. Intense compaction of quartz framework grains also contributed silica. Consequently, quartz cements formed in sandstones during the SBS due to temperature transitions from low to high and localized acidic diagenetic conditions (Fig. 17).

In summary, the E_3h reservoirs in the study area underwent a three-stage burial evolution process: GSS was characterized by mechanical compaction-dominated pore collapse, leading to a rapid decline in the primary pore system. TAS represented a critical period for secondary pore development, establishing the foundation for the reservoir's final configuration and dictating its overall distribution trend. SBS occurred after the overall framework and morphology of the E_3h had been defined. This stage primarily caused regional consolidation of the reservoir, accompanied by localized differential diagenesis. The "coupling" of burial history and diagenetic phases ultimately

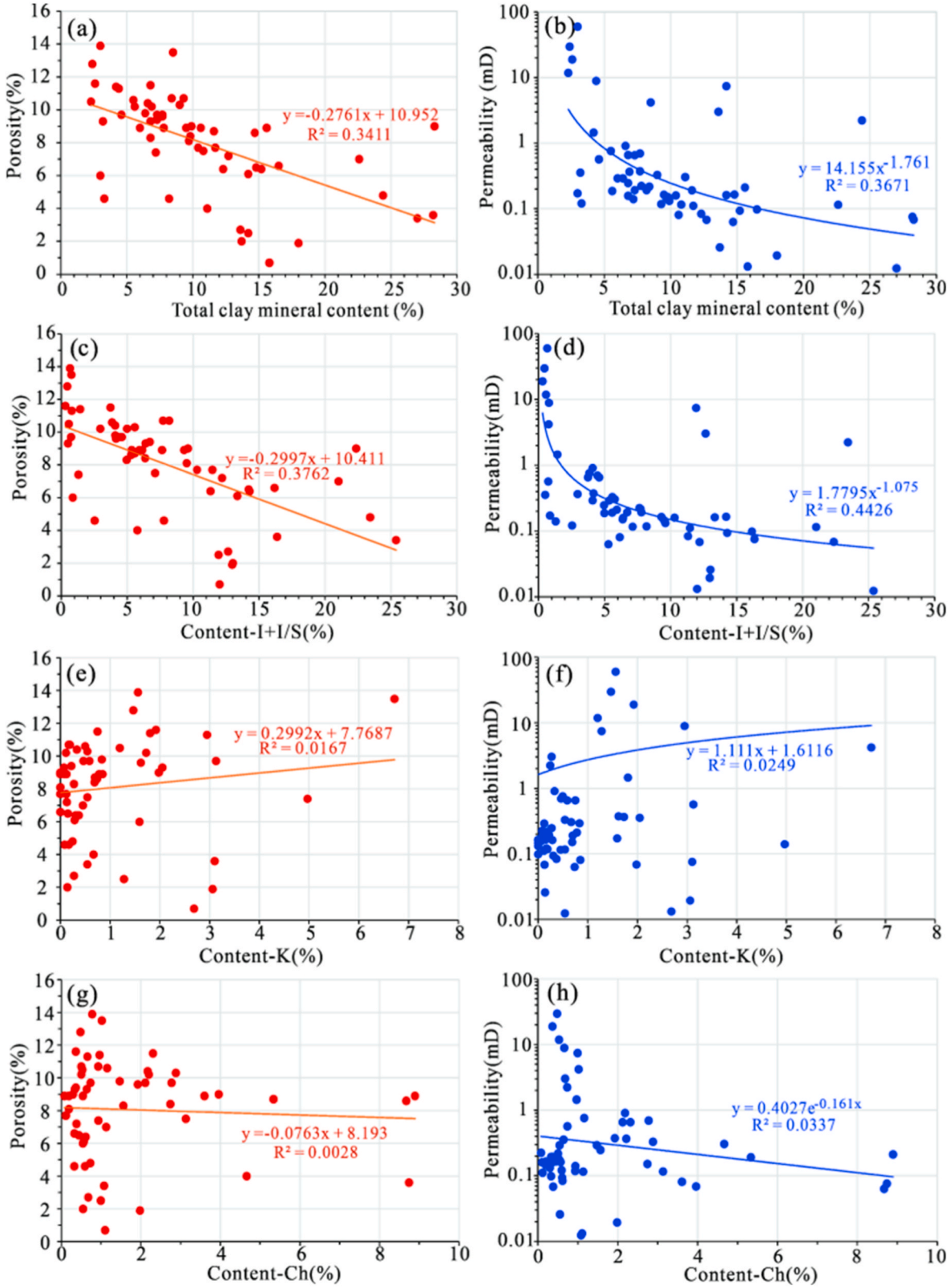

Fig. 16. Relationships between clay minerals and reservoir quality. Crossplots of total clay mineral content (a), (illite + I/S mixed layers) (c), kaolinite (e), and chlorite (g) vs. Porosity. Crossplots of total clay mineral content (b), (illite + I/S mixed layers) (d), kaolinite (f), and chlorite (h) vs. permeability.

determined the current heterogeneous distribution pattern of the reservoir in the study area.

5.3.2. Reservoir quality improvement through sandstone-fault coupling

Previous studies indicate that the study area underwent three major tectonic evolutionary stages: extension-depressional, intense compression, and compressional adjustment, corresponding to three phases of

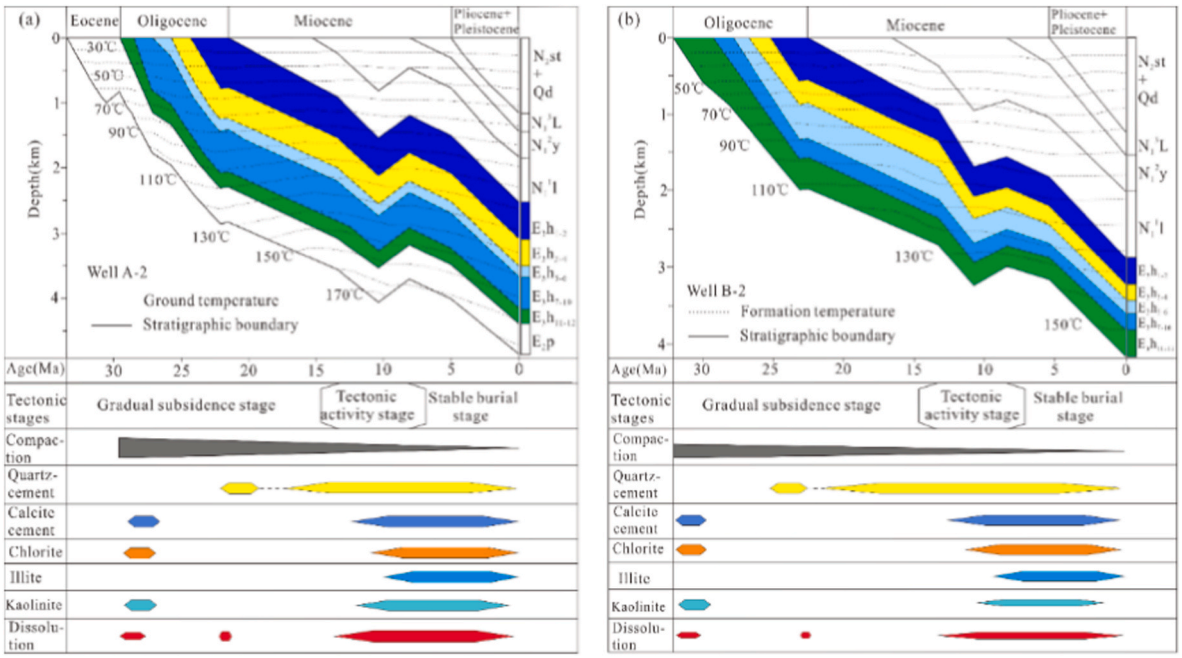

Fig. 17. Coupling relationship between diagenetic sequence and burial history of E_3h sandstones in Wells A-2 (a) and B-2 (b).

fault development.

Stage 1: Early extension to depression (~32–13 Ma). From E_2p deposition (32 Ma) through E_3h and N_1^1l (~13 Ma) periods, the early robust extensional regime transitioned to a depressional phase. Fault activity ceased after the upper E_3h deposition and persisted until N_1^1l (~13 Ma). Faults generated during this interval primarily developed in E_2p and propagated upward into E_3hx (e.g., faults F3, F6, F7). These faults facilitated feldspar dissolution in sandstones within fault zones, generating dissolution pores, while the E_3hs remained largely unaffected.

Stage 2: Intense compression during the early-mid Longjing Movement (13–11 Ma). The Longjing Movement induced intense compression, forming large-scale inversion anticlines and associated adjustment faults (e.g., fault F4). The anticlinal core of the E_3h sandstones experienced significant erosion, enhancing connectivity between sandstones, meteoric water, and underlying acidic fluids via faults and unconformities. This triggered carbonate and feldspar dissolution, forming effective reservoirs. This phase triggered strong dissolution of carbonates and feldspars, forming effective reservoirs. However, in Block B, a weaker tectonic regime resulted in limited faulting in anticlinal cores, restricting fluid connectivity and yielding lower dissolution rates compared to Block A. Fig. 17 demonstrates significantly higher dissolution porosity in Block A reservoirs at 3200–3600 m depths. Seismic interpretation has confirmed that there are numerous small-scale faults in the E_3h sandstones of Well A-2. In contrast, Well B-2 has fewer small-scale faults in its interval, and there is a lack of effective connection with the E_2p source rocks.

Stage 3: Compressional adjustment during the late Longjing Movement (11–8 Ma). Reactivation of the main inversion anticline faults allowed acidic fluids to migrate into sandstones. However, pre-existing dense cementation in the E_3hx sandstones limited dissolution efficacy, resulting in minor reservoir quality improvement.

5.3.3. *Material basis for effective reservoir formation established by high quartz-feldspar provenance*

The provenance characteristics of E_3h sandstone reservoirs, characterized by high quartz (55 %–82 %) and feldspar (10 %–28 %) contents, not only determine the initial mineral composition and structural features of reservoir rocks but also govern the formation and distribution patterns of effective reservoirs through differential responses to subsequent diagenesis.

Deposited in a braided river delta front environment, high-energy hydrodynamic conditions selectively transported fine-grained lithic fragments and clay minerals, while denser, well-rounded quartz and feldspar grains preferentially accumulated (Wang et al., 2021). Well-sorted quartz-feldspar frameworks formed rigid grain-supported structures with initial porosities of 35 %–40 %, establishing a favorable material basis for effective reservoir development. Although significant porosity loss occurred during burial, appreciable intergranular pores persisted (Figs. 13b and. 19a). This maintained permeability during shallow-to-moderate burial, facilitating feldspar dissolution in fault zones. Porosity enhancement from dissolution reduced grain contact stress during inversion tectonism, mitigating pressure solution and preserving reservoir quality. Feldspar content exerts critical controls on compaction resistance, dissolution intensity, and clay mineral cementation. Under early weakly alkaline depositional conditions, feldspar grains synergistically increased reservoir compaction resistance with quartz. However, in acidic diagenetic environments, feldspar dissolution preferentially created secondary porosity. When feldspar dissolution products were not efficiently flushed from reservoirs, authigenic kaolinite and illite formed, partially occluding pores. Overall, high feldspar content benefits effective reservoir formation (Fig. 19b).

The combined effects of sedimentary sorting and diagenetic modification of E_3h quartz-feldspar-rich provenance established the material foundation for reservoir development. The complementary roles of quartz's compaction resistance and feldspar's dissolution susceptibility, dynamically controlled by burial history, ultimately promoted effective reservoir formation.

5.3.4. *Effective reservoir formation model*

Integrating the symbiotic relationships of major diagenetic processes during pore evolution, identification of critical diagenetic periods, fault system characteristics, burial history processes, and impacts of diagenetic processes on reservoir porosity, this study proposes three effective reservoir formation models for the E_3h in the HY area (Fig. 20).

Model I: high dissolution-low cementation-low compaction reservoir development model, characterized by abundant grain-dissolution pores and intergranular pores. During the GSS, mechanical compaction,

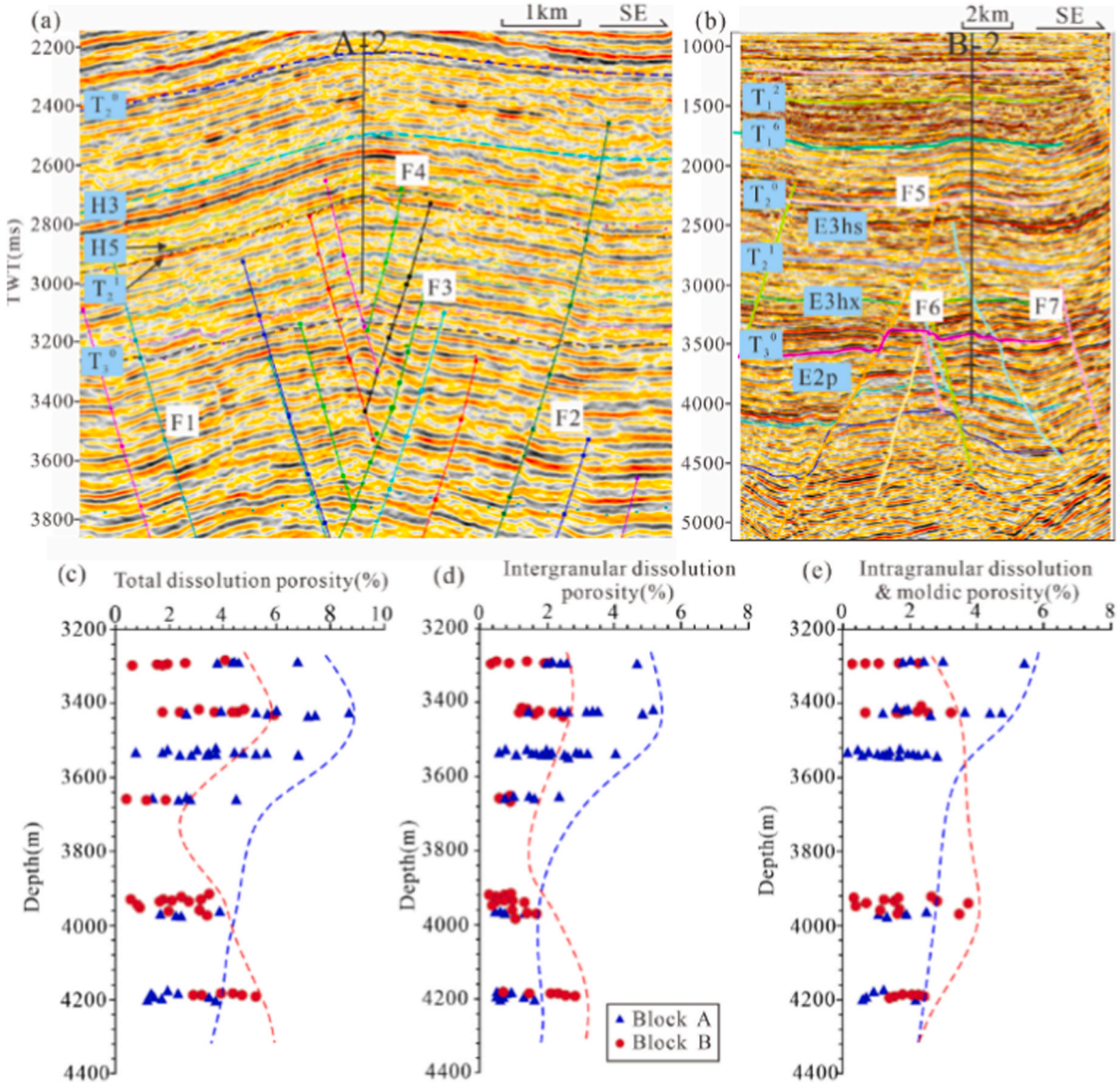

Fig. 18. Fault development characteristics in Blocks A (a) and B (b). Total dissolution pores (c), intergranular dissolution pores (d) and intragranular dissolution & moldic pores (e) variation with depth.

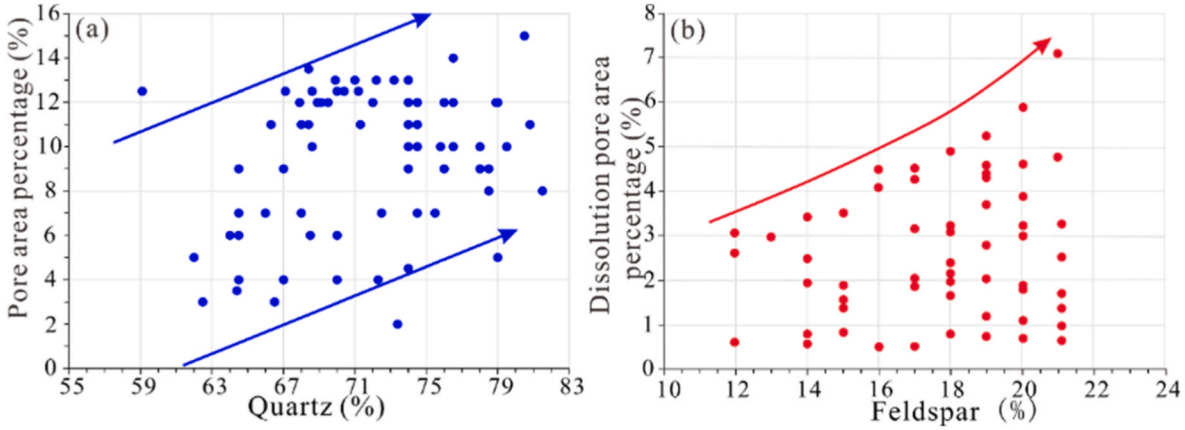

Fig. 19. Crossplots of quartz content vs. pore area percentage (a) and feldspar content vs. dissolution pore area percentage (b) illustrate the positive impact of quartz and feldspar on reservoir quality.

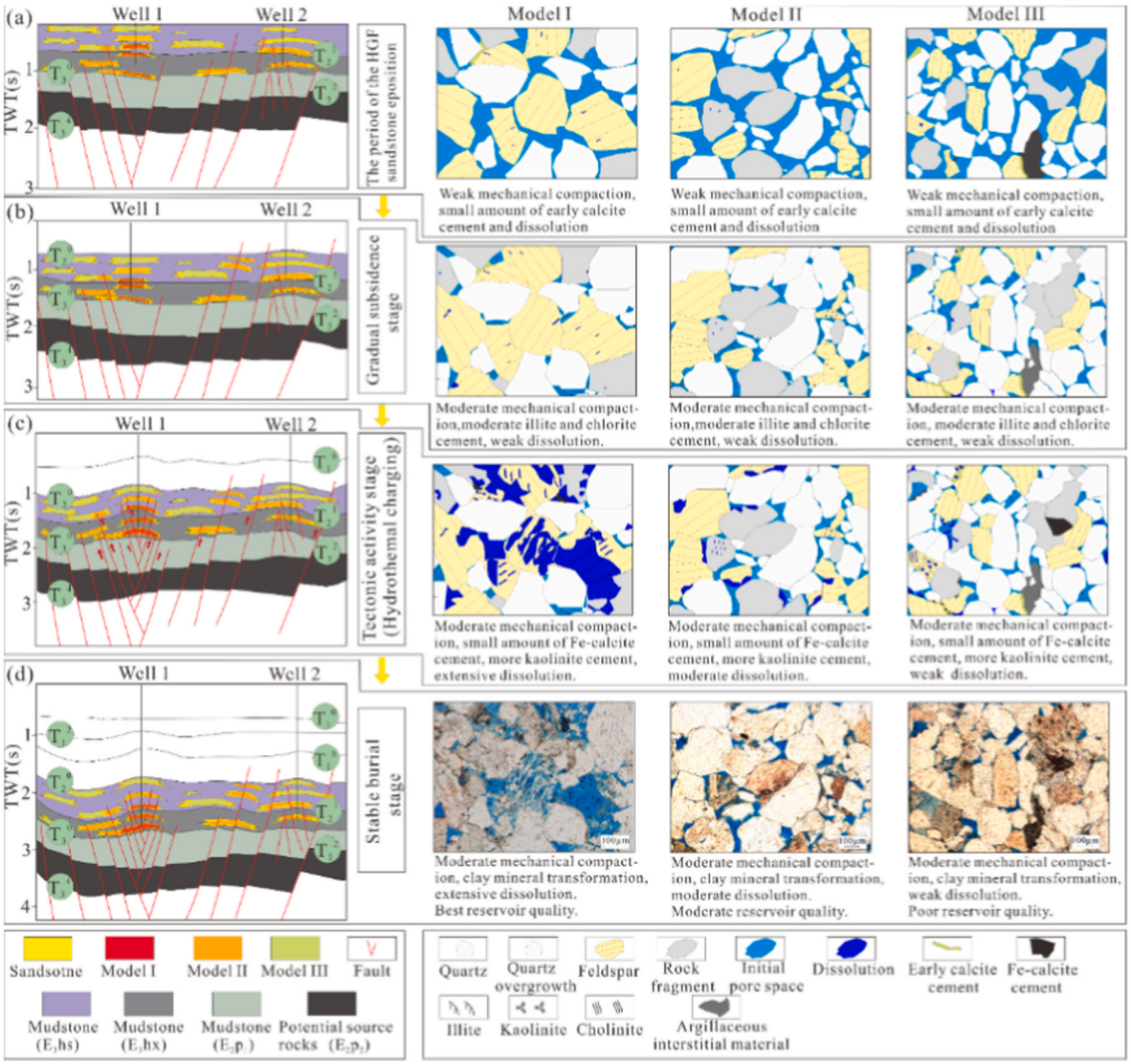

Fig. 20. Tectonic evolution profiles and diagenetic alteration models for effective reservoirs of E_3h sandstones in the HY Area. (a) Reservoir distribution and diagenetic characteristics of sandstones from initial deposition to the end of E_3h deposition period (models I, II, III); (b) Reservoir distribution and diagenetic characteristics at the late period of GSS; (c) Reservoir distribution and diagenetic characteristics at the late period of TAS; (d) Present-day reservoir distribution and diagenetic characteristics after the period of SBS.

carbonate cementation, and siliceous cementation caused significant porosity loss, reducing porosity to ~8.8 %. The TAS witnessed intense tectonic inversion triggered by the Longjing Movement, generating fault networks that uplifted E_3h sandstones and established hydraulic connectivity with acidic fluids from underlying source rocks. This triggered strong dissolution of early carbonate and feldspar cements, forming high-quality reservoirs with ~15 % porosity. Additionally, if faults near sandstones are well connected to the underlying source rocks, acidic fluids would migrate into the rocks, triggering feldspar dissolution during this stage. This process can also form effective reservoirs with porosities approaching 15 %. During the SBS, compaction and clay mineral transformation modified the reservoir, ultimately forming effective reservoirs with current porosities ranging from 12 % to 15 %.

Model II: moderate dissolution-low cementation-low compaction reservoir development model, exhibiting moderate dissolution pores and primary porosity. During late E_3h deposition, tectonic extension created faults extending into the E_3hx in the study area, facilitating minor dissolution in sandstones. During the subsequent GSS, mechanical compaction, carbonate cementation, and siliceous cementation caused significant porosity loss, reducing porosity to <8 %. Subsequent acidic fluid influx during the Longjing movement enabled partial feldspar dissolution, improving porosity to 11 %–12 %. During the SBS, further compaction and clay mineral transformations established current effective reservoirs with ~11 % porosity.

Model III: low compaction-low cementation-low dissolution reservoir development model, characterized by primary intergranular pores as the dominant pore type. Due to the lack of faults connecting to source rocks and having not undergone significant hydrocarbon charging, this type of reservoir lacks the conditions necessary for extensive dissolution to develop. During the burial process, strong compaction reduced the initial porosity. However, high quartz-feldspar content with compaction-resistant mineralogy and low cement content preserved porosities >9 % in localized zones, maintaining storage capacity.

5.4. *Implications for hydrocarbon exploration and development*

The three effective reservoir genetic models established in this study provide an operational theoretical framework for reservoir evaluation of the E_3h in the HY area. A key aspect of this research is its complement to the conventional burial depth-focused diagenesis theory (Morad et al.,

2010), aligning with recent studies (Bjørlykke, 2014; Bah et al., 2023). Through cross-validation using PetroMod thermal history simulations and fluid inclusion thermometry (ranging from 104 to 155.6 °C), the study confirms that the overlapping areas of fault networks and acidic fluid migration pathways during the Tectonic Activity Stage (TAS, 13–8 Ma) (Figs. 18 and 20) serve as the primary zones controlling dissolution-type high-quality reservoirs. In these zones, dissolution pores comprise more than 45 % of the total pore volume. Model III further clarifies that quartz-feldspar-enriched zones (with quartz content exceeding 55 %) can retain over 10 % of residual primary porosity due to their resistance to compaction. This finding provides a material basis for hydrocarbon preservation and revises the traditional understanding in Morad's model (Morad et al., 2010) that burial depth determines reservoir physical properties.

This study develops a target optimization technology for exploration applications by analyzing the relationship between fault density and dissolution porosity during tectonic activity. For instance, in Block A, the fault-dissolution composite zone identified by Model I has a gas production rate of 15×10^4 m^3/d, which significantly enhances accuracy compared to traditional sedimentary facies-based predictions. The two-phase analysis of burial history and diagenesis offers a groundbreaking insight: the fault activation caused by the Late Miocene Longjing Movement accelerated the dissolution peak by approximately 8 Ma in relation to the maximum burial depth. This mechanism of tectonically driven pulsed dissolution introduces a new approach for spatial and temporal predictions of reservoirs in the East China Sea Basin and other similar rift basins. The study has some limitations, including its focus on macroscopic fault characterization without fully incorporating microfracture networks. However, the established three-stage dynamic coupling model has made certain progress by trying to move beyond simply describing diagenetic phenomena to explaining the tectonic-fluid dynamic mechanisms. The proposed effective reservoir formation model provides certain guidance for guiding the exploration of deep and ultra-deep sandstone oil and gas reservoirs.

6. Conclusion

(1) In the HY area, arkoses are the predominantly developed sandstones in the E_3h interval, followed by lithic quartz sandstones and lithic sandstones. The porosity mainly ranges from 2 % to 15.8 %, and the permeability mainly ranges from 0.01 to 100 mD. Pore types mainly include residual intergranular pores, dissolution pores, and intercrystalline pores. The sandstone reservoirs have undergone intense diagenetic modifications, including compaction, cementation (such as clay minerals, carbonates, and siliceous cements), and dissolution.

(2) The diagenetic stages and evolutionary sequence of the E_3h sandstones have been determined. They have successively experienced early weak compaction of rock grains → meteoric water dissolution of feldspar and clasts → early calcite cementation → intense compaction and early quartz overgrowth → massive dissolution of feldspar, carbonate cements, and lithic fragments → late quartz overgrowth → late cementation of fe-carbonate → clay mineral transformation. Currently, the overall diagenetic stage is the early Mesozoic stage A.

(3) Diagenesis is a key factor in the formation and development of matrix pores in reservoirs. Compaction is the main factor leading to the decline in reservoir quality. Cementation of clay minerals and carbonates is another important factor reducing reservoir quality. Dissolution leads to the formation of secondary pores and is crucial for the formation of effective reservoirs.

(4) The influencing factors for the formation of effective reservoirs in the study area have been determined. Among them, the coupling relationship between diagenesis and burial history determines whether a reservoir can be formed. The configuration relationship between faults and sand bodies is a key controlling factor for the development of secondary dissolution pores. The provenance with high quartz and high feldspar components lays the material foundation for reservoir formation.

(5) Three formation models for effective reservoirs of the E_3h have been proposed, including the low compaction-low cementation-high dissolution model, the low compaction-low cementation-moderate dissolution model, and the low compaction-low cementation-low dissolution model. The study shows that combining the burial history and diagenesis of reservoirs can enhance the understanding of the origin and evolution of sandstone reservoirs in similar basins, providing a reference for the prediction of high-quality reservoirs.

CRediT authorship contribution statement

Hong-Liang Huo: Writing – original draft, Software, Resources, Methodology, Investigation. **Cheng-Lin Liu:** Writing – review & editing, Resources, Data curation. **Dao-Wu Huang:** Resources, Funding acquisition. **An-Qi Tian:** Formal analysis, Data curation. **Rizwan Sarwar Awan:** Writing – review & editing, Software. **Hong-Yan Gao:** Data curation. **Chuang-Xin Liu:** Writing – review & editing, Resources. **Xue-Yong Chen:** Software. **Zi-Ye Tian:** Investigation. **Tao-Zheng Yang:** Methodology. **Bin-Bin Liu:** Writing – review & editing. **Chao-Jun Liang:** Writing – review & editing.

Declaration of competing interest

The authors declare that they have no known competing financial interests or personal relationships that could have appeared to influence the work reported in this paper.

Acknowledgments

This research was supported by the National Key Research and Development Program of China (Grant No. 2021YFA071900) and the National Natural Science Foundation of China (Grant No. 41872127). The authors extend sincere gratitude to the Shanghai Branch of China National Offshore Oil Corporation Ltd. (CNOOC) for their valuable assistance. Additionally, we thank the anonymous reviewers and the editor, Lin Ma, for their contributions in enhancing the manuscript.

Data availability

Data will be made available on request.

References

Abbas, A., Zhu, H., Zeng, Z., Zhou, X., 2018. Sedimentary facies analysis using sequence stratigraphy and seismic sedimentology in the paleogene Pinghu formation, Xihu depression, east China sea shelf basin. Mar. Petrol. Geol. 93, 287–297.

Bah, B., Beaudoin, N.E., Lacombe, O., Girard, J., Gout, C., Godeau, N., et al., 2023. Multi-proxy reconstruction of the burial history and porosity evolution of the TOCA carbonate formation in the lower Congo Basin (South West Africa). Mar. Petrol. Geol. 148, 106018.

Baiyegunhi, C., Liu, K., Gwavava, O. & Baiyegunhi, T. L. Diagenesis and reservoir properties of the Permian Ecca group sandstones and mudstones in the Eastern Cape Province, South Africa: implications for the shale gas potential in the Karoo Basin.) 2018 AAPG International Conference and Exhibition.

Behar, F., Vandenbroucke, M., Tang, Y., Marquis, F., Espitalie, J., 1997. Thermal cracking of kerogen in open and closed systems: determination of kinetic parameters and stoichiometric coefficients for oil and gas generation. Org. Geochem. 26, 321–339.

Bello, A.M., Usman, M.B., Amao, A.O., Al-Ramadan, K., Al-Hashem, M., Kachalla, A., et al., 2024. Diagenesis and reservoir quality evolution of estuarine sandstones: insights from the Cenomanian-Turonian Yolde Formation, northern Benue Trough, NE Nigeria. Mar. Petrol. Geol. 169, 107073.

Bjørlykke, K., 2014. Relationships between depositional environments, burial history and rock properties. Some principal aspects of diagenetic process in sedimentary basins. Sediment. Geol. 301, 1–14.

Blamey, N.J., Azmy, K., Brand, U., 2014. Provenance and burial history of cement in sandstones of the Northbrook formation (Carboniferous), western Newfoundland, Canada: a geochemical investigation. Sediment. Geol. 299, 30–41.

Chen, S., Xian, B., Ji, Y., Li, J., Tian, R., Wang, P., et al., 2024. Influences of burial process on diagenesis and high-quality reservoir development of deep-ultra-deep clastic rocks: a case study of Lower Cretaceous Qingshuihe formation in southern margin of Junggar Basin, NW China. Petrol. Explor. Dev. 51, 364–379.
Ehrenberg, S.N., 1989. Assessing the relative importance of compaction processes and cementation to reduction of porosity in sandstones: discussion; compaction and porosity evolution of Pliocene sandstones, Ventura Basin, California: discussion. AAPG Bull. 73, 1274–1276.
El-Ghali, M.A., Shelukhina, O., Abbasi, I.A., Moustafa, M.S., Hersi, O.S., Siddiqui, N.A., et al., 2024. Depositional and sequence stratigraphic controls on diagenesis in the upper cambrian-lower Ordovician Barik formation, central Oman: implications for prediction of reservoir porosity in a hybrid-energy delta system. Mar. Petrol. Geol. 160, 106611.
Faiz, M., Saghafi, A., Sherwood, N., Wang, I., 2007. The influence of petrological properties and burial history on coal seam methane reservoir characterisation, Sydney Basin, Australia. Int. J. Coal Geol. 70, 193–208.
Feng, D., Liu, C., Feng, X., Wang, X., Awan, R.S., Yang, X., et al., 2023. Movable fluid evaluation of tight sandstone reservoirs in lacustrine delta front setting: occurrence characteristics, multiple control factors, and prediction model. Mar. Petrol. Geol. 155, 106393.
Folk, R.L., 1980. Petrology of Sedimentary Rocks. Hemphill publishing company.
Goldstein, J.I., Newbury, D.E., Michael, J.R., Ritchie, N.W., Scott, J.H.J., Joy, D.C., 2017. Scanning Electron Microscopy and X-ray Microanalysis. springer.
Hao, L., Wang, Q., Guo, R., Tuo, C., Ma, D., Mou, W., et al., 2018. Diagenetic fluids evolution of Oligocene Huagang formation sandstone reservoir in the south of Xihu Sag, the East China Sea Shelf Basin: constraints from petrology, mineralogy, and isotope geochemistry. Acta Oceanol. Sin. 37, 25–34.
Higgs, K.E., Zwingmann, H., Reyes, A.G., Funnell, R.H., 2007. Diagenesis, porosity evolution, and petroleum emplacement in tight gas reservoirs, Taranaki Basin, New Zealand. J. Sediment. Res. 77, 1003–1025.
Houseknecht, D.W., 1987. Assessing the relative importance of compaction processes and cementation to reduction of porosity in sandstones. AAPG Bull. 71, 633–642.
Huang, Y., Kane, I.A., Zhao, Y., 2020. Effects of sedimentary processes and diagenesis on reservoir quality of submarine lobes of the Huangliu Formation in the Yinggehai Basin, China. Mar. Petrol. Geol. 120, 104526.
Huo, H., Liu, C., Zhao, A., Li, W., Awan, R.S., Yi, T., et al., 2025. Evaluation of movable fluid and controlling factors in lacustrine gravity-flow tight sandstone reservoirs: implications for predicting reservoir quality. J. Asian Earth Sci. 277, 106374.
Hyodo, A., Kozdon, R., Pollington, A.D., Valley, J.W., 2014. Evolution of quartz cementation and burial history of the Eau Claire formation based on in situ oxygen isotope analysis of quartz overgrowths. Chem. Geol. 384, 168–180.
Irwin, H., Curtis, C., Coleman, M., 1977. Isotopic evidence for source of diagenetic carbonates formed during burial of organic-rich sediments. Nature 269, 209–213.
Keith, M.L., Weber, J.N., 1964. Carbon and oxygen isotopic composition of selected limestones and fossils. Geochem. Cosmochim. Acta 28, 1787–1816.
Lai, J., Wang, G., Fan, Z., Chen, J., Wang, S., Zhou, Z., et al., 2016. Insight into the pore structure of tight sandstones using NMR and HPMI measurements. Energy Fuel. 30, 10200–10214.
Lander, R.H., Laubach, S.E., 2015. Insights into rates of fracture growth and sealing from a model for quartz cementation in fractured sandstones. Bulletin 127, 516–538.
Lander, R.H., Larese, R.E., Bonnell, L.M., 2008. Toward more accurate quartz cement models: the importance of euhedral versus noneuhedral growth rates. AAPG Bull. 92, 1537–1563.
Li, Y., Chen, J., Elsworth, D., Pan, Z., Ma, X., 2022. Nanoscale mechanical property variations concerning mineral composition and contact of marine shale. Geosci. Front. 13, 101405.
Lin, J., Dong, C., Lin, C., Duan, D., Ma, P., Zhao, Z., et al., 2024. The impact of tectonic inversion on diagenesis and reservoir quality of the Oligocene fluvial sandstones: the upper Huagang formation, Xihu Depression, East China Sea Shelf Basin. Mar. Petrol. Geol. 165, 106860.
Liu, J.S., Xu, H.Z., Jiang, Y.M., Wang, J., He, X.J., 2020. Mesozoic and Cenozoic basin structure and tectonic evolution in the East China Sea basin. Acta Geol. Sin. 94, 675–691.
Liu, C., Rong, H., Chen, S., Tang, Y., Deng, Y., 2024. Diagenesis and reservoir property variations of tight sandstone with burial depths ranging from shallow to ultra-deep in the Kuqa depression, Tarim Basin, China. Nat. Gas. Ind. B 11, 121–139.
Ma, X., Yan, W., Yang, Y., Sun, R., Chao, Y., Zhang, G., et al., 2025. Sediment provenance and facies analysis of the Huagang formation in the Y-Area of the central anticlinal Zone, Xihu Sag, East China Sea. J. Mar. Sci. Eng. 13, 520.
Marghani, M.M., Zairi, M., Radwan, A.E., 2023. Facies analysis, diagenesis, and petrophysical controls on the reservoir quality of the low porosity fluvial sandstone of the Nubian formation, east Sirt Basin, Libya: insights into the role of fractures in fluid migration, fluid flow, and enhancing the permeability of low porous reservoirs. Mar. Petrol. Geol. 147, 105986.
Min, L., Hua, C., Xianke, H.E., Yinghui, L., Huang, X., Zhang, X., et al., 2023. Application of seismic sedimentology in characterization of fluvial-deltaic reservoirs in Xihu sag, East China Sea shelf basin. Petrol. Explor. Dev. 50, 138–151.
Morad, S., Al-Ramadan, K., Ketzer, J.M., De Ros, L.F., 2010. The impact of diagenesis on the heterogeneity of sandstone reservoirs: a review of the role of depositional facies and sequence stratigraphy. AAPG Bull. 94, 1267–1309.
Peng, J., Milliken, K.L., Fu, Q., 2020. Quartz types in the Upper Pennsylvanian organic-rich Cline Shale (Wolfcamp D), Midland Basin, Texas: implications for silica diagenesis, porosity evolution and rock mechanical properties. Sedimentology 67, 2040–2064.
Poursoltani, M.R., Gibling, M.R., Pe-Piper, G., 2019. Diagenesis, burial history, and hydrocarbon potential of Cambrian sandstone in the northern continental margin of Gondwana: a case study of the Lalun formation of central Iran. J. Asian Earth Sci. 172, 143–169.
Qian, W., Yin, T., Zhang, C., Tang, H., Hou, G., 2020. Diagenetic evolution of the Oligocene Huagang Formation in Xihu sag, the East China Sea shelf basin. Sci. Rep. 10, 19402.
Qian, W., Sun, Q., Jones, S.J., Yin, T., Zhang, C., Xu, G., et al., 2022. Diagenesis and controlling factors of Oligocene Huagang Formation tight sandstone reservoir in the south of Xihu sag, the East China Sea Shelf Basin. J. Petrol. Sci. Eng. 215, 110579.
Radwan, A.E., Husinec, A., Benjumea, B., Kassem, A.A., Abd El Aal, A.K., Hakimi, M.H., et al., 2022. Diagenetic overprint on porosity and permeability of a combined conventional-unconventional reservoir: insights from the Eocene pelagic limestones, Gulf of Suez, Egypt. Mar. Petrol. Geol. 146, 105967.
Shackleton, N.J., 1987. Oxygen isotopes, ice volume and sea level. Quat. Sci. Rev. 6, 183–190.
Tamburelli, S., Di Giulio, A., Amadori, C., Consonni, A., Ortenzi, A., 2022. New constraint on burial and thermal history of Devonian reservoir sandstones in the Illizi-Ghadames basin (North Africa) through diagenetic numerical modelling. Mar. Petrol. Geol. 145, 105903.
Wang, W., Yue, D., Zhao, J., Li, W., Wang, B., Wu, S., et al., 2019. Diagenetic alteration and its control on reservoir quality of tight sandstones in lacustrine deep-water gravity-flow deposits: a case study of the Yanchang Formation, southern Ordos Basin, China. Mar. Petrol. Geol. 110, 676–694.
Wang, W., Lin, C., Zhang, X., Dong, C., Ren, L., Lin, J., 2020. Effect of burial history on diagenetic and reservoir-forming process of the Oligocene sandstone in Xihu sag, East China Sea Basin. Mar. Petrol. Geol. 112, 104034.
Wang, W., Lin, C., Zhang, X., Dong, C., Ren, L., Lin, J., 2021. Provenance, clastic composition and their impact on diagenesis: a case study of the Oligocene sandstone in the Xihu sag, East China Sea Basin. Mar. Petrol. Geol. 126, 104890.
Wang, W., Lin, C., Zhang, X., Dong, C., Ren, L., Lin, J., 2022. Structural controls on sandstone compaction within the anticline crest and flank: an example from the Xihu Sag, East China Sea Basin. J. Petrol. Sci. Eng. 211, 110157.
Xi, K., Cao, Y., Jahren, J., Zhu, R., Bjørlykke, K., Haile, B.G., et al., 2015. Diagenesis and reservoir quality of the Lower Cretaceous Quantou Formation tight sandstones in the southern Songliao Basin, China. Sediment. Geol. 330, 90–107.
Xi, K., Cao, Y., Liu, K., Wu, S., Yuan, G., Zhu, R., et al., 2019. Diagenesis of tight sandstone reservoirs in the upper Triassic Yanchang formation, southwestern Ordos Basin, China. Mar. Petrol. Geol. 99, 548–562.
Xie, K., Zhu, Y., Si, Q., Huang, F., 2015. Study on kinetics of hydrocarbon generation from Cenozoic Coal Measures of Xihu Depression. Coal Sci. Technol.
Xu, F., Xu, G., Liu, Y., Zhang, W., Cui, H., Wang, Y., 2020. Factors controlling the development of tight sandstone reservoirs in the Huagang Formation of the central inverted structural belt in Xihu sag, East China Sea Basin. Petrol. Explor. Dev. 47, 101–113.
Yang, Wenze, 2023. Study on the Mechanism of Reservoir Quality Differentiation and Distribution Law of Effective Reservoirs in Low-Permeability Tight Gas Reservoirs. China University of Petroleum, Beijing, 001196, 10.27643/d.cnki.gsybu. 2023.
Yang, Y., Huang, Z., Pan, Y., Liu, C., Qu, T., Li, Z., 2024. Hydrocarbon accumulation process and reservoir-forming models of structure A in the central inversion tectonic belt of the Xihu depression, East China Sea basin. Nat. Gas. Ind. B 11, 341–356.
Zeng, F., Dong, C., Lin, C., Wu, Y., Tian, S., Zhang, X., et al., 2021. Analyzing the effects of multi-scale pore systems on reservoir properties—a case study on Xihu depression, East China Sea Shelf Basin, China. J. Petrol. Sci. Eng. 203, 108609.
Zhang, Y., Pe-Piper, G., Piper, D.J., 2015. How sandstone porosity and permeability vary with diagenetic minerals in the Scotian Basin, offshore eastern Canada: implications for reservoir quality. Mar. Petrol. Geol. 63, 28–45.
Zhang, J., Pas, D., Krijgsman, W., Wei, W., Du, X., Zhang, C., et al., 2020. Astronomical forcing of the Paleogene coal-bearing hydrocarbon source rocks of the East China Sea Shelf Basin. Sediment. Geol. 406, 105715.
Zhang, H., Zhang, Z., Tang, W., Li, K., Li, J., Wang, Q., et al., 2022. Burial and exhumation history of Jurassic sedimentary rocks in the southern margin of the Junggar Basin: implications for the growth of the northern Tianshan Mountains. J. Asian Earth Sci. 236, 105339.
Zhang, Q., Wu, X., Radwan, A.E., Wang, B., Wang, K., Tian, H., et al., 2022. Diagenesis of continental tight sandstone and its control on reservoir quality: a case study of the Quan 3 member of the cretaceous Quantou Formation, Fuxin uplift, Songliao Basin. Mar. Petrol. Geol. 145, 105883.
Zhang, X., Zhang, G., Jiang, Y., Cui, M., He, X., 2023. The control of curved faults on structural trap formation: tiantai slope belt, Xihu Sag, East China Sea. Mar. Petrol. Geol. 156, 106464.
Zhou, X., Xu, G., Cui, H., Zhang, W., 2020. Fracture development and hydrocarbon accumulation in tight sandstone reservoirs of the Paleogene Huagang Formation in the central reversal tectonic belt of the Xihu Sag, East China Sea. Petrol. Explor. Dev. 47, 499–512.
Zhu, W., Zhong, K., Fu, X., Chen, C., Zhang, M., Gao, S., 2019. The formation and evolution of the East China Sea Shelf Basin: a new view. Earth Sci. Rev. 190, 89–111.
Zou, W., Yu, Y., Liu, J., Jiang, Y., Tang, X., Chen, S., et al., 2021. Main controlling factors of the central inversional structure belt and the development of Ningbo anticline in Xihu Sag, East China Sea Basin. Acta Pet. Sin. 42, 176.